8 June 2001

ELSEVIER

Chemical Physics Letters 340 (2001) 591–596

CHEMICAL PHYSICS LETTERS

www.elsevier.nl/locate/cplett

A discrete variable representation study of the dynamics of the double proton transfer in bicyclic oxalamidines

Laia Torres, Miquel Moreno *, José M. Lluch

Departament de Química, Universitat Autònoma de Barcelona, Unitat de Quimica Fisica, 08193 Bellaterra, Barcelona, Spain

Received 15 February 2001; in final form 27 March 2001

Abstract

DFT electronic calculations are performed for the double proton transfer in bicyclic oxalamidines 2,2′-bis-(3,4,5,6-tetrahydro-1,3-diazine) (OA6) and 2,2′-bis-(4,5,6,7-tetrahydro-1,3-diazepine) (OA7). Bidimensional potential energy surfaces retaining the characteristics of the stationary points located in the whole potential are built to calculate the vibrational levels through the discrete variable representation (DVR) method. Zero-point tunneling splittings are similar for both systems but for a given energy there are much less tunneling doublets available in OA6, this being the key factor responsible for the different temperature dependence of the rate for the two systems. © 2001 Elsevier Science B.V. All rights reserved.

1. Introduction

Proton transfer reactions are of fundamental interest in chemistry and because of this they have been studied extensively [1,2]. However, most of the studies have dealt with single proton transfers. Some intramolecular prototropic tautomerisms of considerable interest include more than one proton transfer. A very well known system is the double proton transfer in porphyrins and related derivatives [3–6]. On the theoretical side there is also little work on the dynamics of double proton transfers [7] and only electronic (static) calculations have been performed in the last years [8–10]. Very recently Truong et al. [11] has used the variational transition state theory to study this process.

Recently Limbach's group studied some oxalamidines, a model system of porphhyrins [12]. The double proton transfer is depicted in the Scheme. In particular the NMR spectra of 2,2′-bis-(3,4,5,6-tetrahydro-1,3-diazine) (OA6) and 2,2′-bis-(4,5,6,7-tetrahydro-1,3-diazepine) (OA7) were recorded at different temperatures. At the lower range of temperatures the double proton transfer in either OA6 or in OA7 systems was not observed as the tautomerism is too slow as compared with the NMR time scale. At higher temperatures the OA7 NMR spectrum disclosed the double proton transfer taking place at a rate of the order of the NMR time scale. Conversely, the OA6 NMR spectra remained unchanged. This surprising difference between OA6 and OA7 was tentatively attributted to a higher energy barrier in OA6. An important heavy atom reorganization along the process was also noted. These results were partially validated through semiempirical PM3 calculations [13].

* Corresponding author. Fax: +34-93-581-2920.
E-mail address: mmf@klingon.uab.es (M. Moreno).

PII: S0009-2614(01)00449-3

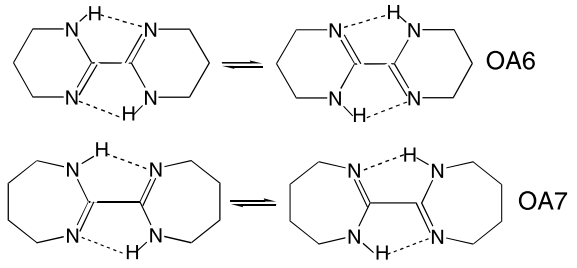

Scheme.

In this Letter we present an electronic (ab initio) + dynamic study to theoretically analyze the double proton transfer in OA6 and OA7.

2. Results and discussion

2.1. Electronic results

DFT calculations were performed with the GAUSSIAN 94 series of programs [14] using the B3LYP method [15] with the 6-31G* basis set [16]. DFT calculations have proven very reliable when dealing with multiple hydrogen bonded systems given energies and geometries at a comparable accuracy with more expensive ab initio techniques [17]. The stationary points were obtained by full geometry optimization [14]. Second derivatives of the energy were calculated analytically and diagonalized to ascertain the nature of each stationary point.

As the double proton-transfer reaction is symmetric, reactant and product geometries are equivalent. Three additional stationary points have been located for each reaction. Fig. 1 depicts all the located structures.

For both OA6 and OA7 systems the equivalent reactant and product configurations (R in Fig. 1) are minima of the potential energy surface (PES). Structure I in Fig. 1 is also a minimum corresponding to a zwitterionic intermediate. It connects with reactant through the transition state (TS in Fig. 1). The transition vector indicates that only one proton is transferring at this stage. Then R, TS and I complete the mechanism for the stepwise double proton transfer: departing from the reactant R a first step involves transfer of one hydrogen through the transition state TS leading to the intermediate I. From here the process follows an equivalent path as the second proton begins to move and a second transition state equivalent to the TS already obtained is passed eventually reaching the product.

In addition, we have also considered the concerted mechanism. We have found the stationary points labeled SP2 in Fig. 1 where both hydrogen atoms are transferring in a synchronous way. These SP2 structures have two imaginary frequencies so that they are not true transition states but saddle points of second order. In this case the two negative eigenvalues correspond to the synchronic and asynchronic motions of both hydrogens. Thus, the concerted R–SP2–R paths are not true reaction paths.

Table 1 presents the relative energies of all these stationary points as well as the imaginary frequencies of transition states and saddle points of second order. The energy barrier as well as the relative energy of the zwitterionic intermediate are lower for the OA7 system. However, the small energy differences between the two oxalamidines do not justify the fact that the double proton transfer is only observed for the OA7 system. In order to gain insight in the mechanism of these reactions, a dynamical study has been undertaken.

2.2. Dynamical results

As quantum dynamical calculations are presently limited to systems with just two or three dimensions, we have constructed analytical two-dimensional PES by fitting the energies and positions of the actual stationary points on the whole PES with the corresponding ones in the reduced two-dimensional PES.

Fig. 2 schematically depicts the PES and the position in this reduced surface of the stationary points obtained on the true multidimensional surface. Fig. 2 corresponds to the OA6 system but the same scheme holds for OA7. Through symmetry considerations the whole surface is divided in four equivalent parts by the x- and y-axis. Motion along the synchronous double proton transfer coincides with the y-axis and passes

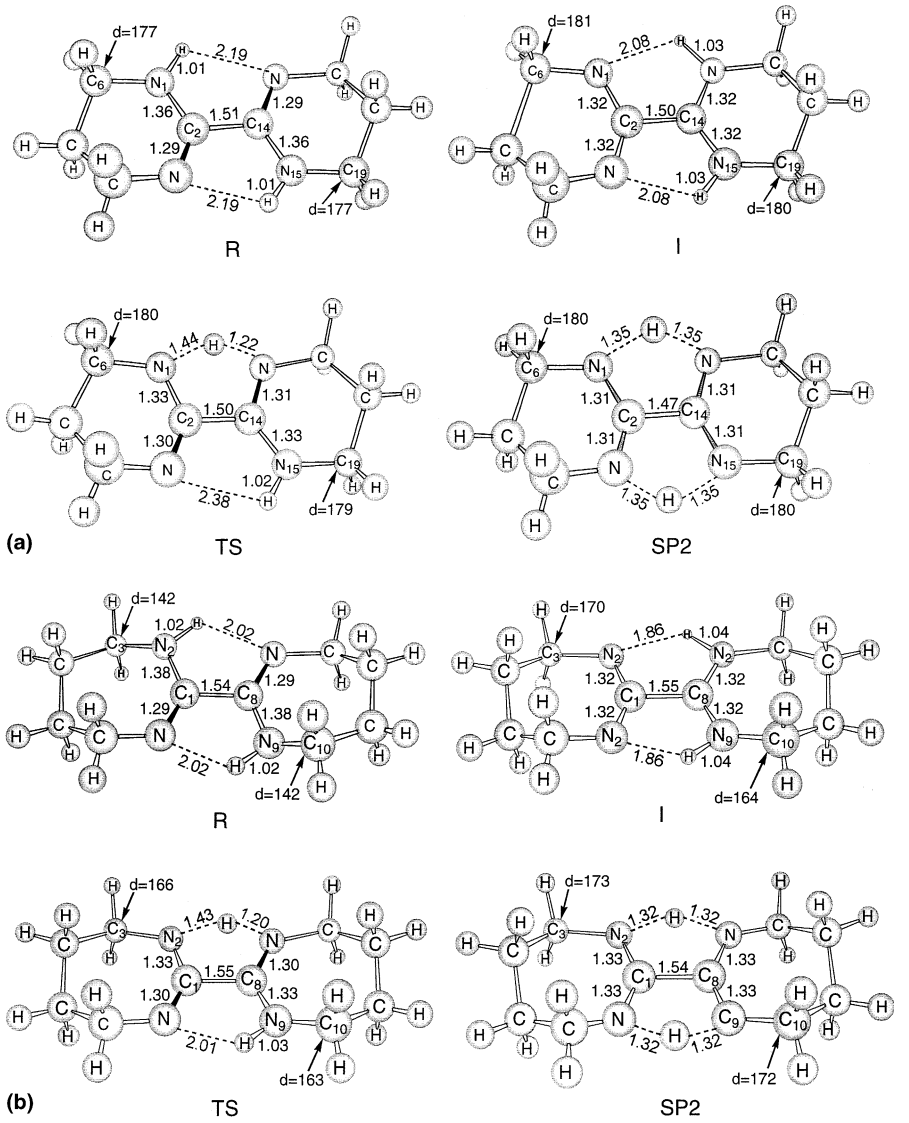

Fig. 1. (a) Geometries of the stationary points located on the potential energy surface for the double proton transfer in the 2,2′-bis-(3,4,5,6-tetrahydro-1,3-diazine) (OA6) system. Bond lengths are given in Å. Dihedral angles in degrees between atoms 6, 1, 2 and 14 and between atoms 19, 15, 14 and 2 are also indicated for each structure; (b) The same for the 2,2′-bis-(4,5,6,7-tetrahydro-1,3-diazepine) (OA7) system.

through the SP2 structure, whereas the stepwise mechanism takes place through one of the two diagonal directions that depart from R and go through one of the two equivalent I geometries. The transition state TS is also located in these diagonals. All these paths are indicated by arrows in Fig. 2.

In previous works we devised a simple analytical potential energy formula to model single proton-transfer reactions [18]. We showed that to correctly model the surface it was necessary to consider the barrier heights and lengths between stationary points. A similar strategy has been used here by fitting a function of the form

Table 1
Energies (in kcal/mol) relatives to reactants of stationary points for the OA6 and OA7 double proton transfer[a]

	OA6	OA7
I	19.6	17.2
TS	24.9 (1305i)	19.8 (1167i)
SP2	45.2 (1842i, 1434i)	29.9 (1718i, 1263i)

[a] Numbers in parentheses correspond to the imaginary frequencies (cm^{-1}) which characterise each stationary point.

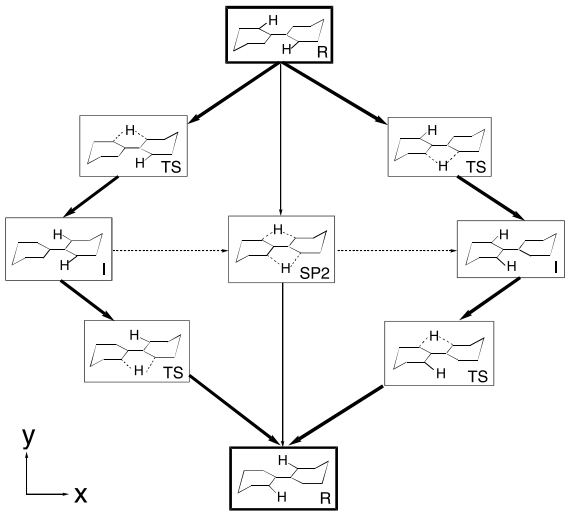

Fig. 2. Schematic localisation of the stationary points for the double proton transfer in the OA6 system in the model two-dimensional potential energy surface. Each stationary point is labeled in accordance with Fig. 1.

$$V(x,y) = -\left(\frac{2B}{A^2}\right)(x^2+y^2) + \left(\frac{B}{A^4}\right)(x^2+y^2)^2.$$

A and B depend on the following parameters obtained from the true multidimensional PES: the rotational angle that measures the rotation of the symmetric one-dimensional double well profile around the energy coordinate, the path length between I and SP2 and between R and SP2 and the energies of the three stationary points. Fig. 3 presents the surface so obtained for OA6. It does not qualitatively differ from the one corresponding to the OA7 system. This way the reduced PES includes the motion of the transferring protons as well as that of the remaining atoms in the molecule.

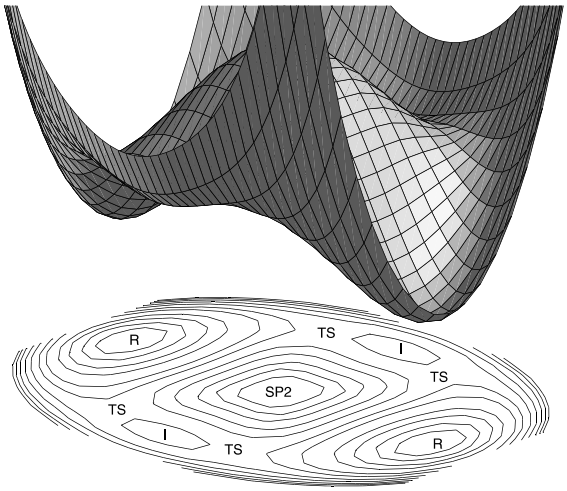

Fig. 3. Three-dimensional picture and contour plot for the model potential energy surface corresponding to the double proton transfer in the OA6 system. Each stationary point is labeled in accordance with Fig. 1.

Next step is to obtain the nuclear (vibrational) stationary states. This has been done through the use of the generic discrete variable representation (DVR) method of Colbert and Miller [19]. As small energy differences are to be measured, the energy levels have to be obtained with high accuracy. In particular we took 3213 and 3283 points for OA6 and OA7 systems, respectively. These were the sizes of the square matrices to deal with. It was verified that a further increase in the number of points did not modify the results.

Table 2 presents the results for some selected levels below the transition state energy for both systems. The first 3 doublets have energies below the intermediate whereas the last doublets energy is above it. Results in Table 2 show that the main difference between the two cases is the vibrational spectrum density, being much greater for the OA7 than for the OA6.

As noted above, the energy barriers for both the stepwise and the concerted path are lower for the OA7 system. This fact alone favors the tunneling for the OA7 system. However tunneling is also strongly dependent on the distance separating the two wells. Table 3 gives the path lengths s along both the stepwise and concerted paths for the two oxalamidines. The distance has been measured by

Table 2
Energies and tunneling splittings of some selected levels for the OA6 and OA7 systems

Doublet	E (kcal/mol)	Δ (cm^{-1})
OA6		
1	2.46	3.28×10^{-10}
11	10.98	6.73×10^{-10}
33	18.75	1.07×10^{-9}
60	24.3	2.54×10^{-2}
OA7		
1	1.27	1.70×10^{-10}
18	7.13	3.17×10^{-10}
77	14.93	1.78×10^{-9}
139	19.7	2.05×10^{-1}

Table 3
Path lengths (in Å $uma^{1/2}$) for the stepwise and concerted OA6 and OA7 double proton transfer

	OA6	OA7
s(R–TS)	2.07	2.6
s(TS–I)	1.85	1.4
s(stepwise)[a]	7.84	8
s(R–SP2)	1.89	3.2
s(concerted)[b]	3.78	6.4

[a] The path length has been calculated as $2(s(\text{R–TS}) + s(\text{TS–I}))$.
[b] The path length has been calculated as $2s(\text{R–SP2})$.

considering the straight-line distances between each consecutive pair of stationary points. It is clear that reaction paths are considerably shorter for the OA6 system so that the two factors governing tunneling act in opposite ways. This explains why the lowest tunneling splitting (which determines the rate constant at low temperature) is quite similar for both systems. The combination of higher barriers and shorter distances makes the potential wells of OA6 considerably narrower so that the energy levels are more separated and, consequently, it is more difficult to populate the excited vibrational levels in OA6 than in the shallower double well of the OA7 system. That is, for the range of energies accessible at a given temperature, there are more energy levels available in the OA7 system. For instance, in the OA7 system there are 9 quasi-degenerated vibrational pairs with energy below 5 kcal/mol with respect to the potential minimum but in OA6 there are only two such a pairs. As a consequence, it is easier to promote the OA7 molecule to higher vibrational levels where the tunneling splitting is higher.

The fact that the path lengths are longer in OA7 may come as a surprise as in OA6 a more extended deformation of the hydrogen bond fragments takes place along the double proton transfer (see the geometrical parameters in Fig. 1). Table 3 reveals that it is in the concerted path where the OA6 path is clearly shorter than the OA7 one. In the stepwise mechanism the difference is considerably reduced. This comes from the shorter distance between R and TS in OA6 being partially compensated by the longer distance from TS to I. The key point is that, in addition to the reorganization of the H-bond fragment (which is larger in the OA6 system), there is a full reorganization of the two rings. This additional reorganization mostly implies motion of the carbon atoms and the hydrogens bound to them in a direction perpendicular to the plane of the double proton transfer so that it can be hardly seen in Fig. 1 (see the dihedral angles in Fig. 1). This motion is not important from an energetic point of view as it mostly implies internal rotations but it accounts for the longer path lengths for the OA7 system as the seven member rings need a considerably larger degree of reorganization to interconvert than the six member ones. This larger flexibility of OA7 can be invoked as a factor favoring energetically the OA7 tautomerism so that both reorganizations (hydrogen bonds fragment and ring deformations) are not independent in these bicyclic systems. Results in Table 3 also indicate that along the stepwise path the ring deformation mainly takes place in the region between the reactant and the transition state whereas between the transition state and the intermediate the nuclear motion can mostly be ascribed to reorganization of the hydrogen bonds.

In conclusion, our dynamical calculations have shown that purely electronic calculations are not enough to understand the different behavior of the two systems when increasing temperature. Zero-point tunneling splitting are small and very similar in both systems. This comes from the fact that the higher energy barrier in OA6 is almost fully compensated by the larger reorganization of the heavy atom skeleton in the OA7 system. This leads to a

clearly longer distance between potential wells in OA7, a factor that slows the tunneling rate. The combination of higher energy barriers and shorter reaction paths leads to narrower potential wells in the OA6 potential energy surface. This implies that the vibrational levels are higher and more separated so that more energy is necessary to appreciably populate vibrational excited levels. This accounts for the fact that tautomerism in OA7 is activated at a lower temperature than OA6. Our dynamical calculations have also demonstrated that the concerted path has to be considered even if it is not a true reaction path.

Acknowledgements

Financial support from the Dirección General de Enseñanza Superior (DGES) through project PB98-0915 is gratefully acknowledged. The use of the computational facilities of the CESCA and CEPBA coordinated by the C^4 are also gratefully acknowledged.

References

[1] Special Issue of Chem. Phys. 136 (1989).
[2] Special Issue of J. Phys. Chem. 95 (1991).
[3] J.R. Reimers, T.X. Lü, M.J. Crossley, N.S. Hush, J. Am. Chem. Soc. 117 (1995) 2855.
[4] J. Braun, H.H. Limbach, P.G. Williams, H. Morimoto, D.E. Wemmer, J. Am. Chem. Soc. 118 (1996) 7231.
[5] O. Brackhagen, Ch. Scheurer, R. Meyer, H.H. Limbach, Ber. Bunsenges. Phys. Chem. 102 (1998) 303 (and references therein).
[6] B. Wehrle, H. Zimmermann, H.H. Limbach, J. Am. Chem. Soc. 110 (1998) 7014.
[7] J.-H. Lim, E.K. Lee, Y. Kim, J. Phys. Chem. A. 101 (1997) 2233.
[8] X.-Y. Li, M.Z. Zgierski, J. Phys. Chem. 95 (1991) 4268.
[9] J. Almlöf, T.H. Fischer, P.G. Gassman, A. Ghosh, M. Häser, J. Phys. Chem. 97 (1993) 10 964.
[10] T.X. Lü, J.R. Reimers, M.J. Crossley, N.S. Hush, J. Phys. Chem. 98 (1994) 11 878.
[11] D.K. Maity, R.L. Bell, T.N. Truong, J. Am. Chem. Soc. 122 (2000) 897.
[12] G. Scherer, H.H. Limbach, J. Am. Chem. Soc. 116 (1994) 1230.
[13] G. Scherer, H.H. Limbach, Croat. Chem. Acta 67 (1994) 431.
[14] M.J. Frisch et al., GAUSSIAN 94, Gaussian Inc., Pittsburgh, PA, 1995.
[15] P. Stephens, F.J. Devlin, C.F. Chabalowski, M.J. Frisch, J. Phys. Chem. 98 (1994) 11 623.
[16] M. Francl, et al., J. Chem. Phys. 77 (1982) 3654.
[17] Q. Zhang, R. Bell, T.N. Truong, J. Phys. Chem. 99 (1995) 592.
[18] E. Bosch, M. Moreno, J.M. Lluch, J. Bertrán, J. Chem. Phys. 93 (1990) 5685.
[19] D.T. Colbert, W.H. Miller, J. Chem. Phys. 96 (1992) 1982.

Nuclear Dynamics Discrete Variable Representation Study of the Equilibrium Isotope Effect on H_2 Binding in $M(\eta^2\text{-}H_2)L_n$ Complexes: An Effective Theoretical Way To Account for Anharmonicity

Laia Torres, Ricard Gelabert, Miquel Moreno, and José M. Lluch*

Departament de Química, Universitat Autònoma de Barcelona, 08193 Bellaterra, Barcelona, Spain

Received: April 6, 2000; In Final Form: June 12, 2000

Equilibrium isotope effects (EIE) on the binding of H_2 and D_2 to transition metal complexes are calculated for a modeled version of $W(CO)_3(PCy_3)_2(\eta^2\text{-}H_2)$, $[Ru(H\cdots H)(C_5Me_5)(dppm)]^+$ and *trans*-$[Os(H\cdots H)Cl(dppe)_2]^+$. Being probably unsatisfactorily described by the harmonic approach (specially in the elongated dihydrogen complexes), the thermodynamic contribution of the H−H stretching related modes is evaluated by means of nuclear motion quantum calculations. The Discrete Variable Representation (DVR) methodology is applied to obtain the anharmonic vibrational spectrum on the bidimensional B3LYP potential surface. From these results, the associated partition function is calculated and used to correct the harmonic EIE and other thermodynamic magnitudes. In agreement with experimental results, the anharmonically corrected EIE for the W complex turns out to be inverse (0.534 at 300 K). On the contrary, the corrected EIE for the Ru and Os complexes is clearly normal (1.217 and 1.685 at 300 K, respectively), predicting an unusual behavior for ML_nH_2 compounds. Comparison with the pure harmonic EIE's leads to the conclusion that the harmonic approach is inadequate to describe the properties of the elongated dihydrogen complexes.

I. Introduction

Isotope effects provide useful information about the molecular properties (structure and reactivity) of the organometallic compounds,[1] specially in fluxional (nonrigid) transition-metal complexes involving dihydrogen or/and hydride ligands. In particular, isotope effects have become a very important tool in the mechanistic study of the reversible oxidative addition of molecular hydrogen to transition-metal complexes, one of the most interesting and characteristic reactions of transition-metal chemistry. Several papers have recently appeared concerning deuterium equilibrium isotope effects (EIE's) for the addition of H_2 and D_2 to various transition-metal complexes in solution to form either metal dihydride/dideuteride complexes[2] or dihydrogen/dideuterium complexes.[3] EIE's are defined as K_H/K_D, where K_H is the equilibrium constant for the perprotio reaction and K_D stands for the equilibrium constant of the isotopically substituted reaction. By definition, an EIE is normal if it is greater than unity, whereas it is inverse if it is less than unity. Observed EIE's for H_2 versus D_2 addition turn out to be usually inverse,[4] with typical values of K_H/K_D around 0.50 or less, showing that metal complexes bind D_2 better than they do H_2 over a large temperature range.

Of special interest is the very recent study[4] of the EIE on H_2 binding to the dihydrogen complex $W(CO)_3(PCy_3)_2(\eta^2\text{-}H_2)$, one of the so-called Kubas complexes (the first isolable dihydrogen complexes). In that paper Bender, Kubas, Hoff and co-workers use the measured vibrational frequencies arising from the corresponding infrared spectra to obtain the molecular translational, rotational and vibrational partition functions ratios as described in the general treatment of equilibrium isotope effects by Bigeleisen and Goeppert-Mayer.[5] From their calculations they get a modest inverse EIE value of 0.78 at 300 K. In addition, by comparison of the equilibrium constants for displacement of N_2 by H_2 or D_2 in the complex $W(CO)_3(PCy_3)_2(N_2)$ in THF solution they obtain an EIE value of 0.70 ± 0.15 at 295 K. At first glance these results seem counterintuitive because the large decrease in the H−H (D−D) stretching frequency due to the H_2 (D_2) binding to the complex should produce a large normal EIE. However, Bender, Kubas, Hoff and co-workers show that the contributions of the five new vibrational modes that appear in the addition product (coming from the original five translational and rotational degrees of freedom in the free hydrogen molecules) overcome the normal contributions of the H−H (D−D) stretching mode and the translational and rotational degrees of freedom, this way leading to an overall inverse EIE.

At this point, an inverse deuterium EIE seems the rule rather than the exception for the addition of molecular hydrogen to suitable metal complexes to form either dihydride or dihydrogen transition-metal complexes. However, we wondered what the EIE would be for the formation of the particular group of transition-metal dihydrogen complexes known as elongated dihydrogen complexes.[6] These complexes fill the gap between classical polyhydrides (with H−H distances at or above 1.6 Å) and nonclassical dihydrogen complexes (which have H−H distances below 1.0 Å). Some of us[7a,b] have recently used a combined electronic Density Functional Theory plus nuclear dynamics study of two complexes to prove that the existence and several properties of the elongated dihydrogen complexes can be explained taking into account the quantum vibrational motion of the hydrogen nuclei on a very anharmonic potential energy surface.

The first purpose of this paper is to theoretically study the deuterium equilibrium isotope effect for the addition of molecular hydrogen to a complex leading to an elongated dihydrogen transition-metal complex. To this aim we will calculate the equilibrium constants of the several equilibria of the type pictured in Scheme 1. Concretely, we will study the EIE corresponding to the formation of the elongated dihydrogen

10.1021/jp001327p CCC: $19.00
Published on Web 08/01/2000

SCHEME 1

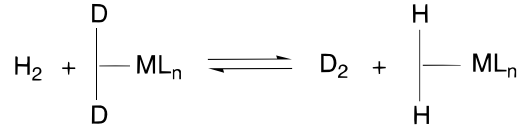

complexes $[Ru(H\cdots H)(C_5Me_5)(dppm)]^+$ and *trans*-$[Os(H\cdots H)Cl(dppe)_2]^+$ (dppm = bis(diphenylphosphino)methane; dppe = 1,2-bis(diphenylphosphino)ethane). For the sake of comparison, the case corresponding to the formation of the dihydrogen complex $W(CO)_3(PCy_3)_2(\eta^2\text{-}H_2)$ will also be considered. On the other hand, it has to be emphasized that, as mentioned above, the interesting properties of the elongated dihydrogen complexes arise from the high anharmonicity of the H−H stretching and that the related vibrational modes are very sensitive to it. As a consequence, any theoretical calculation of the EIE for these complexes should include vibrational anharmonicity in a reliable way. So, the second purpose of this paper is to devise an effective strategy which allows for the practical calculation of the anharmonic vibrational levels that influence the EIE in dihydrogen transition-metal complexes, so that the vibrational partition functions (and the EIE) can be reliably computed at a reasonable cost.

II. Calculational Details

As stated in the Introduction, this work is devoted to obtain equilibrium isotope effects. To this aim we have used a statistical thermodynamic formulation[8] as described in the next section. The molecular partition functions were first computed within the ideal gas, rigid rotor, and harmonic oscillator models. Then a treatment to introduce anharmonicity was employed. A pressure of 1 atm and a temperature of 300 K have been assumed in all the calculations. Two different types of quantum results are required. Electronic structure calculations provide the geometry of the minimum energy structures and permits to build up a sizable part of the potential energy surface (PES). Nuclear motion calculations have been carried out to determinate vibrational (anharmonic) energy levels and their associated vibrational wave functions. Some technical details of both sets of calculations follows.

A. Electronic Structure Calculations. For saving computational effort some modeling has been made on the experimental complexes. The three cyclohexyl groups in the Kubas complex were changed by three hydrogen atoms; the C_5Me_5 unit and the four phenyl groups in the dppm ligand were substituted by a cyclopentadienyl and four hydrogen atoms, respectively, in the ruthenium complex; finally, in the osmium complex the four phenyl groups in the dppe ligand were changed by four hydrogen atoms. As a result the dihydrogen complexes that have actually been studied are $W(CO)_3(PH_3)_2(\eta^2\text{-}H_2)$, $[Ru(H\cdots H)(C_5H_5)(H_2PCH_2PH_2)]^+$ and *trans*-$[Os(H\cdots H)Cl(H_2PCH_2CH_2PH_2)_2]^+$.

All electronic structure calculations have been carried out with the GAUSSIAN 98 series of programs.[9] To solve the electronic Schrödinger equation, the density-functional theory (DFT)[10] methodology has been used. This methodology meets the requirements of high accuracy and reasonable cost, and has been employed with great success to study several organometallic systems, including dihydrogen and polyhydride complexes.[7a,7b,11] The three-parameter hybrid functional of Becke and the Lee, Yang and Parr's correlation functional, widely known as Becke3LYP,[12] have been used.

To reduce the cost of the computations an effective core operator has been used to replace the 60 innermost electrons of the tungsten atom in the Kubas complex. For the 14 outer electrons of the metal atom the basis set was that associated with the pseudopotential of Hay and Wadt[13] with a standard valence double-ξ LANL2DZ contraction.[14] The basis set for the hydrogen atoms directly attached to the metal was a double-ξ supplemented with a polarization p shell.[15,16] A 6-31G basis set[15] was used for the H atoms attached to a P or a C atom, as well as for carbon and oxygen atoms. The phosphorus atoms were described with the 6-31G(d) basis set.[17]

Most of the electronic results for the two elongated dihydrogen complexes have been taken from our previous papers.[7a,7b,18] However, a few new electronic calculations have been carried out for these two complexes using the same level of calculation described there. That is, an effective core operator replacing the inner electrons (28 and 60 in the ruthenium and osmium atoms, respectively), and the basis set associated with the pseudopotential of Hay and Wadt[13] with a standard valence double-ξ LANL2DZ contraction[14] for the 16 outer electrons in both ruthenium and osmium atoms.The basis set for the hydrogen atoms directly attached to the metal was a double-ξ supplemented with a polarization p shell.[15,16] A 6-31G basis set[15] was used for the H atoms attached to a P or a C atom, as well as for carbon atoms. The phosphorus atoms were described with the 6-31G(d) basis set.[17] For the chlorine atom in the osmium complex a 6-31G(d) basis set[17] was used. Finally, a 6-31G(p) basis set was used for the free hydrogen molecule whose geometry has been optimized.

The Z-matrices of the minimum energy structures corresponding to the Kubas complex and the elongated dihydrogen complexes have been obtained from the authors of the ref 19 and from our previous results, respectively.[7a,b] Geometry optimizations have been performed using the Schlegel gradient optimization algorithm using redundant internal coordinates.[14,20]

For each minimum energy structure analytical second derivatives of the energy with respect to the Cartesian coordinates have been computed to obtain the frequencies and eigenvectors associated with each vibrational normal mode within the harmonic approximation. For complexes described by means of pseudopotentials this is a new feature included in GAUSSIAN 98.[9] For those systems GAUSSIAN 94[14] and previous versions only allow numerical second derivatives calculation by finite differences of analytically computed first derivatives, this way involving very time-consuming calculations. The fact that all the frequencies turn out to be real confirms that the located points are actual minima of the PES.

The normal modes have been recalculated for each dideuterated minimum energy structure in order to obtain the frequencies and eigenvectors corresponding to the isotopically substituted species.

B. Nuclear Motion Calculations. As explained in the next section, introducing the anharmonicity effects in the elongated dihydrogen transition-metal complexes requires the solution of the nuclear Schrödinger equation (vibrational energy levels and wave functions) over a suitable PES built up from electronic calculations. Concretely, we have chosen a two-dimensional PES as a function of the interatomic distance between the two hydrogen (deuterium) atoms of the H_2 (D_2) unit of the complex and the distance between the metal atom and the point halfway between those two hydrogen (deuterium) atoms. These two parameters behave as orthogonal coordinates, in such a way that no coupled terms between them appear in the nuclear kinetic operator of the corresponding nuclear Schrödinger equation, that is,

$$\hat{T} = \frac{-\hbar^2}{2\mu_x}\frac{\partial^2}{\partial x^2} + \frac{-\hbar^2}{2\mu_y}\frac{\partial^2}{\partial y^2} \quad (1)$$

where x and y stand for the H−H and M−H_2 distances, respectively.

When calculating the PES, global relaxation of the rest of geometrical parameters has been allowed. Some additional details concerning the PES are given in the next section.

To solve the nuclear Schrödinger equation a discrete variable representation (DVR)[21,22] has been used. This method has already been applied with success in the field of organometallic chemistry.[7] Computationally, the DVR has great advantages over the more traditional variational basis representation, in which the energy levels are obtained by diagonalization of the matrix representation of the projection of the Hamiltonian operator on a given basis set. In short, the DVR is a grid-point representation instead of a basis set representation, and thus it facilitates the calculation of the potential energy integrals V_{ij}. In this representation, the potential energy matrix is diagonal,

$$V_{ii'} = \delta_{ii'}V(x_i) \quad (2)$$

and the kinetic energy matrix is very simple,

$$T_{ii'} = \frac{\hbar^2(-1)^{i-i'}}{2m\Delta x^2}\begin{cases} \pi^2/3 & i = i' \\ \dfrac{2}{(i-i')^2} & i \neq i' \end{cases} \quad (3)$$

leading to a very sparse Hamiltonian matrix easier to diagonalize than those coming from a basis set representation,

$$H_{ij,i'j'} = T_{ii'}\delta_{jj'} + T_{jj'}\delta_{ii'} + \delta_{ii'}\delta_{jj'}V(x_i, y_j) \quad (4)$$

In this paper the generic DVR proposed by Colbert and Miller[22] has been used. Once the grid-point representation of the nuclear Hamiltonian has been built up, the nuclear energy levels and wave functions are found through diagonalization of this matrix. The nuclear wave functions Ψ_i are obtained as a linear combination of associated basis functions ϕ_j

$$\Psi_i = \sum_{j=1}^{N_p} c_{ij}\phi_j \quad (5)$$

where N_p is the total number of points in the grid. In a general two-dimensional case whose two dimensions are labeled x and y, ϕ_j are functions of the form

$$\phi_j(x, y) = \frac{\sin\left(\dfrac{\pi(x - x_m)}{\Delta x}\right)}{\pi(x - x_m)} \cdot \frac{\sin\left(\dfrac{\pi(y - y_m)}{\Delta y}\right)}{\pi(y - y_m)} \quad (6)$$

being x_m and y_m the (x, y) coordinates of the grid point associated with the basis function ϕ_j, and Δx and Δy the spacings in the x and y directions of the grid. The wave function has to be normalized prior to any calculation involving it.

III. Results and Discussion

According to the well-known formulas of the statistical thermodynamics,[8] we will calculate the deuterium equilibrium isotope effect as the equilibrium constant (K_H/K_D) of the equilibrium displayed in Scheme 1. For the three cases studied in this work ML_n stands for $W(CO)_3(PH_3)_2$, $[Ru(C_5H_5)(H_2PCH_2PH_2)]^+$ and *trans*-$[OsCl(H_2PCH_2CH_2PH_2)_2]^+$.

A. Harmonic EIE. First of all, within the harmonic approximation, we have used the molecular partition functions provided by GAUSSIAN 98 for each chemical species in Scheme 1 to evaluate the harmonic EIE's. In addition, we have decomposed each EIE as the product of three factors: the translational-rotational contribution (TRANSROT); the factor corresponding to the contribution of the ground vibrational states, that is, only including the zero-point energy levels (ZPE); and the factor that appears when the excited vibrational energy levels are taken into account (EXC). The corresponding results are shown in Table 1. Our harmonic EIE for the complex $W(CO)_3(PH_3)_2(\eta^2\text{-}H_2)$ turns out to be inverse, although numerically is somewhat lesser (that is to say, the isotope effect turns out to be more intense) than the value calculated by Bender, Kubas, Hoff and co-workers[4] from the infrared spectra. The difference stems fundamentally from the ZPE factor, which is the main responsible of the inverse behavior. On the other hand, the complexes $[Ru(H\cdots H)(C_5H_5)(H_2PCH_2PH_2)]^+$ and *trans*-$[Os(H\cdots H)Cl(H_2PCH_2CH_2PH_2)_2]^+$ also give inverse harmonic EIE's, with figures that do not qualitatively differ from those corresponding to the Kubas complex. Then, our theoretical results seem to confirm the inverse deuterium EIE as a rule for the formation of the transition-metal dihydrogen complexes, at least within the harmonic approximation.

B. Anharmonic EIE. We wondered what the effect of the anharmonicity on the EIE's would be, specially for the elongated dihydrogen complexes. Theoretical harmonic vibrational frequencies are, in general, overestimated[23] because of incomplete incorporation of electron correlation, the use of finite basis sets and, as a major source of error, the neglect of anharmonicity effects. For this reason, scaling factors are often applied prior to the use of the frequencies in the EIE calculations. Scaling factors for obtaining fundamental vibrational frequencies, low-energy vibrations, zero-point vibrational energies and thermal contributions to enthalpy and entropy from theoretical harmonic frequencies have been determined by Scott and Radom[24] by fitting to experimental values. To our knowledge, no scaling factors have been explicitly developed for calculating isotope effects through vibrational partition functions. Perhaps the scaling factors recommended for the prediction of the zero-point vibrational energies or the thermochemical quantities, at the Becke3LYP/6-31G(d) level, could be appropriate (0.9806, 0.9989, and 1.0015 for the zero-point vibrational energies, the thermal contribution to enthalpy and the thermal contribution to entropy, respectively).[24] Note that in this formalism we are looking for anharmonically corrected frequencies that provide good results when used in the harmonic expression of the vibrational partition function. As a matter of fact this is the approach adopted by Bender, Kubas, Hoff and co-workers[4] when introducing the measured vibrational frequencies from the infrared spectra (and so including anharmonicity) in the harmonic treatment of Bigeleisen and Goeppert-Mayer.[5] However, we decided not to use any scaling factors in this paper for two reasons. First of all, the above indicated scaling factors are very close to one and they do not appreciably modify the calculated EIE's indicated in Table 1. Second, those scaling factors have not been fitted to reproduce properties of transition metal complexes and even less to account for the high degree of anharmonicity found in the elongated dihydrogen complexes.

Instead of calculating anharmonically corrected frequencies, in the present paper we will try to determine directly the anharmonic vibrational energy levels. Assuming an independent normal-mode framework (i.e., no mode−mode coupling), the vibrational partition function of the molecule is separable as a

TABLE 1: Harmonic EIE's and Contributions to Them

	$W(CO)_3(PH_3)_2(\eta^2\text{-}H_2)$	$[Ru(H\cdots H)(C_5H_5)(H_2PCH_2PH_2)]^+$	*trans*-$[Os(H\cdots H)Cl(H_2PCH_2CH_2PH_2)_2]^+$
TRANSROT	5.519 (5.77)	5.470	5.553
ZPE	0.131 (0.20)	0.135	0.189
EXC	0.675 (0.67)	0.729	0.665
EIE	0.486 (0.78)	0.538	0.696

Numbers in parentheses correspond to the values calculated by Bender, Kubas, Hoff and co-workers from the infrared spectra.

product of the contributions corresponding to each individual normal mode. The potential energy along a single mode could be expanded in a series of powers of the associated normal coordinate with coefficients given by the second, third, fourth and higher numerical directional derivatives of the potential energy along the normal-mode direction. If the vibrational energy levels E_i^m of the one-dimensional potential energy along the mode m can be determined in some way, the vibrational partition function for mode m (q_m) can be calculated as

$$q_m = \sum_i e^{-E_i^m/k_B T} \tag{7}$$

where k_B is the Boltzmann's constant. To avoid the calculation of high numerical derivatives (with the associated lack of accuracy) it is better to build up a one-dimensional potential energy surface as a function of each normal coordinate. Then we can solve the nuclear Schrödinger equation by means of the DVR method to find the vibrational energy levels, which incorporate the anharmonicity associated with each normal mode in a natural way.

Our three dihydrogen transition-metal complexes have between 17 and 28 nuclei, what implies dealing with 45−78 vibrational normal modes. Application of the above outlined procedure to each normal mode is a task out of reach. Instead, to account for the anharmonicity in a practical way, we propose an attainable strategy that works in the following fashion:

(a) The most anharmonic vibrational normal modes are previously chosen (they will be called anharmonic modes from here on).

(b) For each anharmonic normal mode a one-dimensional PES as a function of the corresponding normal coordinate is built up.

(c) The DVR method is used to solve the nuclear Schrödinger equation over the PES associated with each anharmonic normal mode, therefore obtaining the corresponding anharmonic vibrational energy levels.

(d) The anharmonic vibrational partition function for each anharmonic normal mode is computed through eq 7.

(e) The anharmonic vibrational partition function of the molecule is calculated as a product of the anharmonic vibrational partition functions corresponding to the anharmonic normal modes and the harmonic vibrational partition functions corresponding to the remaining normal modes (the ones that can be considered harmonic modes). As a matter of fact, this is done by substituting the original harmonic contributions of the anharmonic modes in the totally harmonic vibrational partition function of the molecule by their corresponding anharmonic vibrational partition functions.

What are the main sources of anharmonicity in the dihydrogen transition-metal complexes that can influence the EIE's? Indeed they will be associated with the dihydrogen ligand. Owing to the large mass difference between the light hydrogen (or deuterium) nuclei and the heavy rest of the complex, the normal modes involving the hydrogen (or deuterium) nuclei consist fundamentally of their motion. There are 6 such vibrational modes.[4] The associated normal coordinates can be defined from

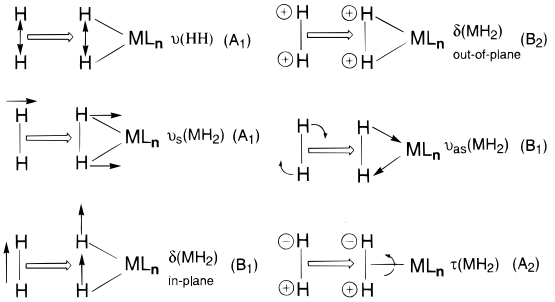

Figure 1. Symmetry coordinates associated with the dihydrogen ligand along with their irreducible representation in a C_{2v} symmetry point group. For the three cases studied in this work ML_n stands for $W(CO)_3(PH_3)_2$, $[Ru(C_5H_5)(H_2PCH_2PH_2)]^+$ and *trans*-$[OsCl(H_2PCH_2CH_2PH_2)_2]^+$.

suitable displacement coordinates adapted to symmetry, which are pictured in Figure 1. These symmetry coordinates correspond to the unique vibrational mode (the H−H stretching) and the lost translational and rotational degrees of freedom for free hydrogen. Assuming that the hydrogen nuclei move under the field of a heavy point center (ML_n) formed by the rest of the complex, their symmetry point group is C_{2v}. Figure 1 also shows the irreducible representation to which each symmetry coordinate belongs. There are two totally symmetrical coordinates (A_1), two coordinates with symmetry species B_1, one B_2 symmetry coordinate and one A_2 symmetry coordinate. Each normal coordinate has to be a linear combination of the symmetry coordinates that belong to the same irreducible representation of this normal coordinate. For instance, the normal coordinates of the two A_1 modes are linear combination of the two A_1 symmetry coordinates (the H−H stretching and the symmetric $M-H_2$ stretching).

The major anharmonicity effect is probably related to the H−H stretching (specially for the elongated dihydrogen complexes), which participates in the two A_1 normal modes. Then both A_1 normal modes have to be considered as anharmonic modes in the sense defined above. In addition, it is expected that anharmonicity couples significantly the two modes of the same symmetry. Therefore, we will assume the independent normal-mode framework neglecting all the mode−mode couplings but the coupling between the two A_1 modes, that will not be separated in our treatment. This assumption slightly modifies the above introduced a−e working scheme, in the sense that both anharmonic normal modes are studied together over a two-dimensional PES as a function of the two symmetry coordinates that define the corresponding normal coordinates. This leads to a two-dimensional anharmonic vibrational partition function that will substitute the two original one-dimensional harmonic contributions of the anharmonic modes in the harmonic vibrational partition function of the molecule, in this way leading to the anharmonic vibrational partition function of the molecule.

A series of electronic structure calculations have been performed to construct the two-dimensional PES for the complex $W(CO)_3(PH_3)_2(\eta^2\text{-}H_2)$. A collection of 120 points, each corresponding to a different set of H−H and $W-H_2$ distances, has

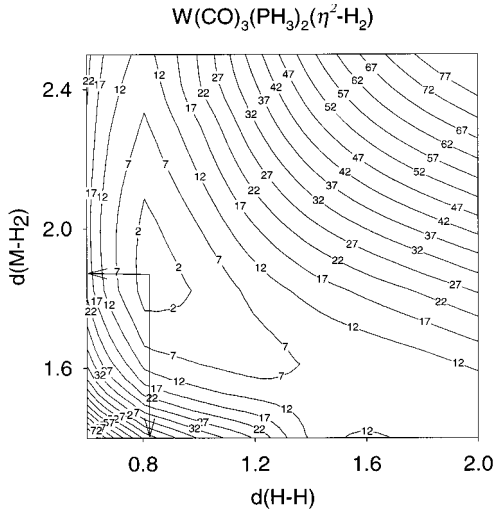

Figure 2. Contour plot of the two-dimensional potential energy surface for the complex $W(CO)_3(PH_3)_2(\eta^2\text{-}H_2)$. Distances are given in Å. Energy contours appear every 5 kcal/mol. The arrows indicate the position of the minimum energy structure (d(H−H) = 0.832 Å and d(M−H_2) = 1.872 Å).

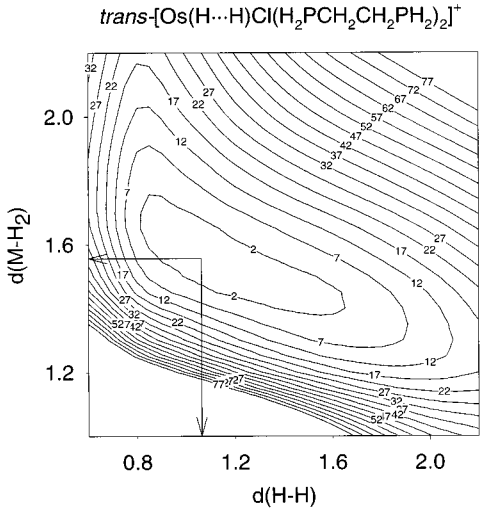

Figure 3. Contour plot of the two-dimensional potential energy surface for the complex *trans*-$[Os(H\cdots H)Cl(H_2PCH_2CH_2PH_2)_2]^+$. Distances are given in Å. Energy contours appear every 5 kcal/mol. The arrows indicate the position of the minimum energy structure (d(H−H) = 1.071 Å and d(M−H_2) = 1.567 Å).

been calculated. The ranges covered have been from 0.6 to 2.0 Å for the H−H distance, and from 1.4 to 2.5 Å for the distance between the tungsten atom and the midpoint halfway between the two hydrogen atoms. The resulting points have been fitted into a two-dimensional cubic splines functional form,[25] which is a smooth and continuous function. Figure 2 depicts the two-dimensional PES as a contour plot.

Analogous two-dimensional PES′ were built up for the two elongated dihydrogen complexes in two previous papers.[7a,b] For the complex $[Ru(H\cdots H)(C_5H_5)(H_2PCH_2PH_2)]^+$ the range for the H−H distance covered from 0.59 to 2.29 Å, while the Ru−H_2 distance covered from 1.00 to 2.20 Å. As for the complex *trans*-$[Os(H\cdots H)Cl(H_2PCH_2CH_2PH_2)_2]^+$, the intervals were from 0.6 to 2.2 Å and from 1.0 to 2.2 Å for the H−H and the Os−H_2 distances, respectively. From those two works we have borrowed the corresponding fitted two-dimensional cubic splines. The PES′ for the complexes $[Ru(H\cdots H)(C_5H_5)(H_2PCH_2PH_2)]^+$ and *trans*-$[Os(H\cdots H)Cl(H_2PCH_2CH_2PH_2)_2]^+$ turn out to be qualitatively similar and for the sake of conciseness only the second one has been pictured in Figure 3.

Comparison between Figures 2 and 3 discloses important differences. The first one concerns to the position of the minimum energy structure. For the Kubas complex it is found at d(H−H) = 0.832 Å and d(W−H_2) = 1.872 Å, whereas the corresponding values of the minimum energy structure for the complex *trans*-$[Os(H\cdots H)Cl(H_2PCH_2CH_2PH_2)_2]^+$ are 1.071 and 1.567 Å, respectively. However, the most important point is the shape of the PES in the region next to the minima. Around the minimum energy structure of the Kubas complex, a normal dihydrogen complex, the potential energy valley is quite parallel to the W−H_2 axis with a trend to curve along the H−H direction as the W−H_2 distance shortens (Figure 2). As a consequence, the two normal modes of A_1 symmetry, although mixed to some extent (as already pointed out by Bender, Kubas, Hoff and coworkers[4]), can be still identified, respectively, with the two A_1 symmetry coordinates. That is to say, one normal mode is basically the H−H stretching and the other one is essentially the symmetric M−H_2 stretching. This is, probably, a common feature of the normal dihydrogen transition-metal complexes. The scenario for the *trans*-$[Os(H\cdots H)Cl(H_2PCH_2CH_2PH_2)_2]^+$ clearly differs (Figure 3). In this case the potential energy valley surrounding the minimum energy structure is oblique, in such a way that none of the two A_1 normal modes can be identified at all with one of the A_1 symmetry coordinates depicted in Figure 1. Along the normal mode that is roughly parallel to the energetically smooth oblique valley, the stretching of the H−H bond leads to shortening of the M−H_2 distance, and vice versa. On the other hand, the other normal mode is orthogonal to the first one and consists of the simultaneous stretching (or compression) of both the H−H bond and the M−H_2 distance. Apart from the obliqueness of the two A_1 normal modes that imposes a global treatment, this valley is highly anharmonic, this being a crucial factor in determining the interesting properties of the elongated dihydrogen transition metal-complexes.

Once the two-dimensional cubic splines that define the PES′ have been obtained, the corresponding nuclear Schrödinger equations can be solved using the DVR method. First of all, a certain reduced mass has to be assigned to each degree of freedom in the Hamiltonian. As in our previous works,[7a,b,18] the reduced masses for the motion along the symmetry coordinates have been calculated (for the perprotio complexes) as

$$\frac{1}{\mu_{d(H-H)}} = \frac{1}{m_{H(A)}} + \frac{1}{m_{H(B)}}$$

$$\frac{1}{\mu_{d(M-H_2)}} = \frac{1}{m_{H_2}} + \frac{1}{m_{[ML_n]}} \qquad (8)$$

Note that the reduced masses of the dideuterated complexes can be calculated in an analogous way. Then, the matrix representation of the nuclear Hamiltonian over a rectangular grid of equally spaced points has been constructed. Different sizes of each grid have been tested until convergence of the energy levels has been achieved. The characteristics of the final grids chosen for the different systems have been as follows: 35 × 27 = 945 for both the perprotio and the dideuterated complexes $W(CO)_3(PH_3)_2(\eta^2\text{-}H_2)$; 29 × 21 = 609 for both the perprotio and the dideuterated complexes $[Ru(H\cdots H)(C_5H_5)(H_2PCH_2PH_2)]^+$; and 33 × 25 = 825 and 37 × 27 = 999 for the perprotio and the dideuterated complexes *trans*-$[Os(H\cdots H)Cl(H_2PCH_2CH_2PH_2)_2]^+$, respectively (the format used is: number of points along the H−H coordinate × number of points

TABLE 2: Anharmonic EIE's (see text) and Contributions to Them

	$W(CO)_3(PH_3)_2(\eta^2\text{-}H_2)$	$[Ru(H\cdots H)(C_5H_5)(H_2PCH_2PH_2)]^+$	*trans*-$[Os(H\cdots H)Cl(H_2PCH_2CH_2PH_2)_2]^+$
TRANSROT	5.519	5.470	5.553
ZPE	0.143	0.323	0.505
EXC	0.676	0.689	0.601
EIE	0.534	1.217	1.685

TABLE 3: Thermodynamic Functions (300 K) Corresponding to the Equilibria of the Type Pictured in Scheme 1[a]

	$W(CO)_3(PH_3)_2(\eta^2\text{-}H_2)$		$[Ru(H\cdots H)(C_5H_5)(H_2PCH_2PH_2)]^+$		*trans*-$[Os(H\cdots H)Cl(H_2PCH_2CH_2PH_2)_2]^+$	
	har	anhar	har	anhar	har	anhar
ΔH^b	0.906	0.871	0.912	0.350	0.688	0.041
ΔS^c	1.587	1.663	1.806	1.555	1.584	1.157
ΔG^b	0.431	0.373	0.370	−0.117	0.216	−0.314

[a] Har and Anhar stand for the Harmonic and Anharmonic aproximations, respectively. [b] In kcal·mol^{-1}. [c] In cal·mol^{-1}·K^{-1}

along the M−H_2 coordinate = total number of points). Diagonalization of the corresponding 6 matrices provides the 6 sets of vibrational wave functions (eigenvectors) and anharmonic energy levels (eigenvalues). These energy levels permit the calculation of the anharmonic vibrational partition function of each molecule according to the procedure outlined above and then the anharmonic EIE's are obtained.

Table 2 exhibits the anharmonic EIE's and their decomposition in factors (evidently the TRANSROT contribution is the same as in Table 1). Comparison of Tables 1 and 2 shows that anharmonicity does not significantly alter the EXC factor. The important changes only concern the ZPE factor. For the complex $W(CO)_3(PH_3)_2(\eta^2\text{-}H_2)$ anharmonicity augments just slightly the ZPE contribution and, therefore, the EIE. The anharmonic EIE, still clearly inverse, is somewhat closer to the experimental values than the harmonic EIE. Taking into account the range of uncertainty of the experimental values[4] (0.78 from infrared spectra or 0.70 ± 0.15 from displacement of N_2) and that anharmonicity has been only partially incorporated, the agreement is rather good. Anyway, we have shown that anharmonicity tends to favor the addition of H_2. This effect is magnified in the two highly anharmonic elongated dihydrogen complexes. The anharmonic EIE's for the complex $[Ru(H\cdots H)(C_5H_5)(H_2PCH_2PH_2)]^+$ and, specially, for the complex *trans*-$[Os(H\cdots H)Cl(H_2PCH_2CH_2PH_2)_2]^+$ (even more anharmonic than the complex of ruthenium) become clearly normal. Then, we predict theoretically that the deuterium equilibrium isotope effect for the addition of molecular hydrogen to a transition-metal complex leading to the formation of $[Ru(H\cdots H)(C_5H_5)(H_2PCH_2PH_2)]^+$ or *trans*-$[Os(H\cdots H)Cl(H_2PCH_2CH_2PH_2)_2]^+$ is clearly normal. That is to say, H_2 binds better than D_2 to both $[Ru(C_5H_5)(H_2PCH_2PH_2)]^+$ and $[OsCl(H_2PCH_2CH_2PH_2)_2]^+$, and this conclusion is probably general for the formation of any elongated dihydrogen transition metal complex.

Why anharmonicity tends to favor the addition of H_2? Isotopic substitution by deuterium lowers the vibrational energy levels corresponding to normal modes that consist fundamentally of motion of hydrogen nuclei, that is, the 6 normal modes associated with the dihydrogen ligand (Figure 1). The key is that the larger the anharmonicity of the normal modes sensitive to the isotopic substitution in the dihydrogen complex, the smaller the gap between the equivalent HH and DD vibrational energy levels. Along the addition, the change in the HH/DD zero-point energy gap for the normal mode corresponding originally to the H−H (D−D) stretching in the free hydrogen molecule gives a normal ZPE factor (a value greater than unity). This effect is larger as the HH/DD gap is smaller in the dihydrogen complex. On the contrary, conversion of the 5 translational and rotational modes in free hydrogen to vibrational normal modes in the dihydrogen complex leads to an inverse ZPE factor (a value smaller than unity), this effect being smaller as the HH/DD gap is more reduced in the dihydrogen complex. As a consequence of all this, anharmonicity increases the numerical values of the ZPE factors associated with the dihydrogen ligand (the normal and inverse factors become more normal and less inverse, respectively), so tending to produce a normal EIE. This effect is so important in the highly anharmonic elongated dihydrogen transition-metal complexes that the EIE becomes normal.

Finally, we have to remark that the anharmonic corrections calculated in this paper are based on a two-dimensional approach. Indeed, this reduction of dimensionality is a limitation. However, the results obtained at the 2D approximation sounds reasonable. As a matter of fact, the major source of anharmonicity is related with the H−H stretching, which participates in the two A_1 normal modes. Given the size of the systems, inclusion of more dimensions (B_1 normal modes) would be out of reach. On the other hand, incorporation of coupling would be desireable but it is not probably necessary in order to obtain a reasonable prediction that can be useful for experimentalists.

C. Thermodynamic Functions. We have calculated the thermodynamic functions at 300 K corresponding to the equilibria of the type pictured in Scheme 1. The harmonic values are obtained from the harmonic molecular partition functions according to the suitable statistical thermodynamic formulas.[8] We have determined the anharmonic values by substituting in the corresponding expressions the contributions of the two original one-dimensional harmonic vibrational partition functions of the two anharmonic modes by the contribution of the two-dimensional anharmonic vibrational partition function. Results are shown in Table 3. Note that ΔH also gives the reaction enthalpy difference ($\Delta\Delta H$) between the addition of H_2 to a transition-metal complex leading to the formation of a dihydrogen complex and the corresponding addition of D_2. The same is true for the entropy and the Gibbs energy.

For the complex $W(CO)_3(PH_3)_2(\eta^2\text{-}H_2)$ it is clear that, as already found by Bender, Kubas, Hoff and co-workers,[4] D_2 binding is enthalpically favored over H_2 binding, but it is disfavored entropically. Anharmonic values are somewhat closer to the experimental thermodynamic functions (ΔH = 0.64 kcal mol^{-1} and ΔS = 1.7 cal mol^{-1} K^{-1}), the agreement being excellent. Our corresponding EIE's (see above) have been apparently not so good in comparison with the experimental results, but it has to be recalled that EIE's are measured as equilibrium constants, that is, as exponential functions of ΔG and, indeed, they are much more sensitive to small errors (theoretical or experimental). On the other hand, anharmonicity lowers the endothermicity of equilibria indicated in Scheme 1

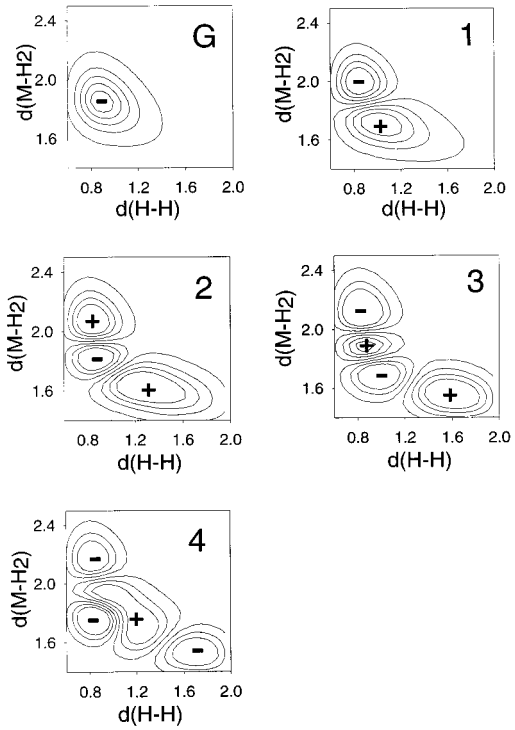

Figure 4. Contour plots of the vibrational wave functions associated with the ground vibrational state (G) and the first (1), second (2), third (3) and fourth (4) excited states for the complex $W(CO)_3(PH_3)_2(\eta^2\text{-}H_2)$. Distances are given in Å. (+) and (−) refer to the sign of the vibrational wave function in order to indicate where the nodes are.

because it also reduces the gap among the equivalent HH and DD vibrational energy levels in the dihydrogen complexes. This effect is again highly amplified in the two elongated dihydrogen complexes, for which that endothermicity becomes quite small (only when anharmonicity is introduced). In these cases the entropic term ($-T\Delta S$) dominates at this temperature and the EIE becomes normal. It becomes manifest that anharmonicity is cleary required to describe correctly the thermodynamic of the process for the elongated dihydrogen transition-metal complexes.

D. Anharmonic Vibrational Wave Functions. A final point concerns the anharmonic vibrational wave functions obtained as eigenvectors of the DVR matrices. For the sake of brevity, we will only comment the vibrational wave functions corresponding to the perprotio complexes $W(CO)_3(PH_3)_2(\eta^2\text{-}H_2)$ and *trans*-$[Os(H\cdots H)Cl(H_2PCH_2CH_2PH_2)_2]^+$. Figures 4 and 5 present the contour plots of the wave functions associated with the ground vibrational state and the first excited states for both the Kubas complex and the elongated dihydrogen complex, respectively. The ground wave function spreads on the low-energy basin around the minimum energy structure on the PES. Conversely, excited wave functions tend to progressively expand toward higher energy regions. As a matter of fact the wave functions reflect the shape of the corresponding PES. So, the ground wave function for the Kubas complex surrounds rather symmetrically the minimum (compare Figures 2 and 4), showing a slight deviation along the H−H direction as the $W-H_2$ distance shortens. The wave functions associated with the first, second and third excited states present one, two and three nodal lines, respectively. These states are all vibrationally excited states corresponding to progressive excitations of the normal mode that is basically the $W-H_2$ stretching which is the direction with smoothest slope around the minimum on the PES. However, the progressive expansion of the excited wave

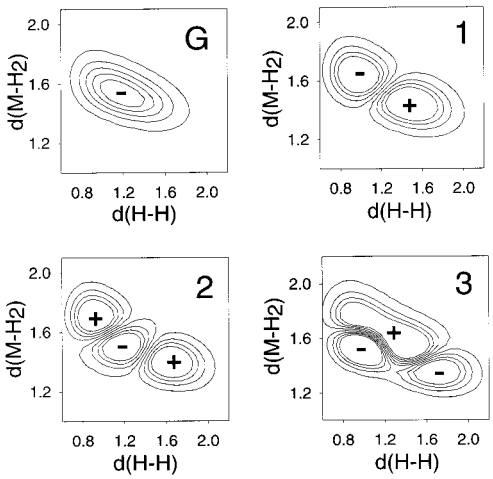

Figure 5. Contour plots of the vibrational wave functions associated with the ground vibrational state (G) and the first (1), second (2) and third (3) excited states for the complex *trans*-$[Os(H\cdots H)Cl(H_2PCH_2\text{-}CH_2PH_2)_2]^+$. Distances are given in Å. (+) and (−) refer to the sign of the vibrational wave function in order to indicate where the nodes are.

functions along the H−H direction suggests that the symmetric $W-H_2$ stretching normal mode mixes more and more with the H−H stretching normal mode as the order of the excitation grows. On the other hand, the fourth excited state displays only one (although somewhat sinuous) nodal line and corresponds to the first excitation of the H−H stretching normal mode (the steepest direction around the minimum on the PES). In this case an important mixing with the symmetric $W-H_2$ stretching normal mode is present as indicated by the expansion of the wave function along the $W-H_2$ direction.

The scenario is different for the complex *trans*-$[Os(H\cdots H)\text{-}Cl(H_2PCH_2CH_2PH_2)_2]^+$. In this case, the ground and the excited wave functions spread along the energetically smooth, long oblique valley (compare Figures 3 and 5). The first and second excited states possess one and two nodal lines, respectively, roughly perpendicular to the major axis of the almost elliptic valley. These states are vibrationally excited states corresponding to progressive excitations of the normal mode roughly parallel to the valley. On the other hand, the third excited state has only one nodal line approximately along the major axis of the valley and corresponds to the first excitation of the second A_1 normal mode (the one that vibrates along the steepest direction). It has to be underlined that, for the elongated dihydrogen complexes, the degree of coupling between both A_1 normal modes does not seem to change as the order of the excitation goes up, at least for the lower excited states analyzed here.

IV. Conclusions

In this paper we have theoretically calculated the deuterium equilibrium isotope effect for the binding of H_2 and D_2 to three dihydrogen transition-metal complexes: $W(CO)_3(PCy_3)_2(\eta^2\text{-}H_2)$, $[Ru(H\cdots H)(C_5Me_5)(dppm)]^+$ and *trans*-$[Os(H\cdots H)Cl(dppe)_2]^+$. Concretely, we have taken the complexes $W(CO)_3(PH_3)_2(\eta^2\text{-}H_2)$, $[Ru(H\cdots H)(C_5H_5)(H_2PCH_2PH_2)]^+$ and *trans*-$[Os(H\cdots H)\text{-}Cl(H_2PCH_2CH_2PH_2)_2]^+$, respectively, as realistic models of them. The last two complexes are known to be elongated dihydrogen complexes for which the high anharmonicity related to the H−H stretching is a crucial feature that determines many of their special properties. In this paper, we propose an attainable strategy to account for the effects of anharmonicity in a practical and reliable way. In short, the procedure consists of using a

discrete variable representation to solve the nuclear Schrödinger equation on the potential energy surface built up along the most anharmonic vibrational normal modes. This provides the corresponding anharmonic vibrational energy levels and, from them, an anharmonically corrected vibrational partition function of the molecule can be calculated. This partition function is not the complete anharmonic partition function of the molecule yet, but it contains the anharmonicity contributions corresponding to the considered modes.

We have proven, within the pure harmonic approach, that an inverse deuterium equilibrium isotope effect is found for the three complexes. However, anharmonicity tends to favor the H_2 binding. Anharmonicity in the complex $W(CO)_3(PH_3)_2(\eta^2\text{-}H_2)$ is not important enough to change the preference for D_2 binding (in good agreement with the experimental results), but the deuterium equilibrium isotope effect is clearly normal for the binding in $[Ru(H\cdots H)(C_5H_5)(H_2PCH_2PH_2)]^+$ and *trans*-$[Os(H\cdots H)Cl(H_2PCH_2CH_2PH_2)_2]^+$. This is the first time that the preference for the binding of H_2 is predicted in elongated dihydrogen transition-metal complexes. This result opens new possibilities to separate hydrogen isotopes at room temperature on metal complexes that reversibly bind molecular hydrogen so that experimental work devoted to proving that theoretical prediction would be very interesting

Finally, it has to be emphasized that anharmonicity has to be taken into account in order to reproduce and theoretically predict the experimental results concerning many properties of dihydrogen and, probably, polyhydride transition-metal complexes, specially in what concerns the isotope effects. Since experimental results in this field are not easy to obtain, we think that the theoretical procedure we propose here can be very useful to clarify many related problems as, for instance, whether deuterium favors a classical versus a nonclassical site in transition metal complexes. Work on this topic is now in progress in our laboratory.

Acknowledgment. The authors thank Professor Agustí Lledós and his group for providing some electronic information about the Kubas complex. Financial support from DGES through project PB98-0915 and the use of the computational facilities of the CESCA and CEPBA coordinated by the C^4 are also gratefully acknowledged.

References and Notes

(1) Bullock, R. M. In *Transition Metal Hydrides*; Dedieu, A., Ed.; VCH Publishers: New York, 1992; p 263.

(2) (a) Hostetler, M. J.; Bergman, R. G. *J. Am. Chem. Soc.* **1992**, *114*, 7629. (b) Rabinovich, D.; Parkin, G. *J. Am. Chem. Soc.* **1993**, *115*, 353. (c) Abu-Hasanayn, F.; Krogh-Jespersen, K.; Goldman, A. S. *J. Am. Chem. Soc.* **1993**, *115*, 8019.

(3) (a) Gusev, D. G.; Bakhmutov, V. I.; Grushin, V. V.; Vol'pin, M. E. *Inorg. Chim. Acta* **1990**, *177*, 115. (b) Hauger, B. E.; Gusev, D. G.; Caulton, K. G. *J. Am. Chem. Soc.* **1994**, *116*, 208. (c) Bakhmutov, V. I.; Bertrán, J.; Esteruelas, M. A.; Lledós, A.; Maseras, F.; Modrego, J.; Oro, L. A.; Sola, E. *Chem. Eur. J.* **1996**, *2*, 815.

(4) Bender, B. R.; Kubas, G. J.; Jones, L. H.; Swanson, B. I.; Eckert, J.; Capps, K. B.; Hoff, C. D. *J. Am. Chem. Soc.* **1997**, *119*, 9179.

(5) Bigeleisen, J.; Goeppert-Mayer, M. *J. Chem. Phys.* **1947**, *15*, 261.

(6) (a) Jessop, P. J.; Morris, R. H. *Coord. Chem. Rev.* **1992**, *121*, 155. (b) Brammer, L.; Howard, J. A. K.; Johnson, O.; Koetzle, T. F.; Spencer, J. L.; Stringer, A. M. *J. Chem. Soc., Chem. Commun.* **1991**, 241. (c) Albinati, A.; Bakhmutov, V. I.; Caulton, K. G.; Clot, E.; Eckert, J.; Eisenstein, O.; Gusev, D. G.; Grushin, V. V.; Hauger, B. E.; Klooster, W. T.; Koetzle, T. F.; McMullan, R. K.; O'Louhlin, T. J.; Pélissier, M.; Ricci, J. S.; Sigalas, M. P.; Vymenits, A. B. *J. Am. Chem. Soc.* **1993**, *115*, 7300. (d) Hasegawa, T.; Li, Z.; Parkin, S.; Hope, H.; McMullan, R. K.; Koetzle, T. F.; Taube, H. *J. Am. Chem. Soc.* **1994**, *116*, 4352. (e) Klooster, W. T.; Koetzle, T. F.; Jia, G.; Fong, T. P.; Morris, R. H.; Albinati, A. *J. Am. Chem. Soc.* **1994**, *116*, 7677. (f) Maltby, P. A.; Schlaf, M.; Steinbeck, M.; Lough, A. J.; Morris, R. H.; Klooster, W. T.; Koetzle, T. F.; Srivastava, R. C. *J. Am. Chem. Soc.* **1996**, *118*, 5396. (g) Heinekey, D. M.; Luther, T. A. *Inorg. Chem.* **1996**, *35*, 4396. (h) Earl, K. A.; Jia, G.; Maltby, P. A.; Morris, R. H. *J. Am. Chem. Soc.* **1991**, *113*, 3027.

(7) (a) Gelabert, R.; Moreno, M.; Lluch, J. M.; Lledós, A. *J. Am. Chem. Soc.* **1997**, *119*, 9840. (b) Gelabert, R.; Moreno, M.; Lluch, J. M.; Lledós, A. *J. Am. Chem. Soc.* **1998**, *120*, 8168. (c) Scheurer, C.; Wiedenbruch, R.; Meyer, R.; Ernst, R. R.; Heinekey, D. M. *J. Chem. Phys.* **1996**, *106*, 1. (d) Maseras, F.; Lledós, A.; Clot, E.; Eisenstein, O. *Chem. Rev.* **2000**, *100*, 601.

(8) McQuarrie, D. A. *Statistical Thermodynamics*; University Science Books: Mill Valley, CA, 1973.

(9) Frisch, M. J.; Trucks, G. W.; Schlegel, H. B.; Scuseria, G. E.; Robb, M. A.; Cheeseman, J. R.; Zakrzewski, V. G.; Montgomery, J. A.; Stratmann, R. E.; Burant, J. C.; Dapprich, S.; Millam, J. M.; Daniels, A. D.; Kudin, K. N.; Strain, M. C.; Farkas, O.; Tomasi, J.; Barone, V.; Cossi, M.; Cammi, R.; Mennucci, B.; Pomelli, C.; Adamo, C.; Clifford, S.; Ochterski, J.; Petersson, G. A.; Ayala, P. Y.; Cui, Q.; Morokuma, K.; Malick, D. K.; Rabuck, A. D.; Raghavachari, K.; Foresman, J. B.; Cioslowski, J.; Ortiz, J. V.; Stefanov, B. B.; Liu, G.; Liashenko, A.; Piskorz, P.; Kamaromi, I.; Gomperts, R.; Martin, R. L.; Fox, D. J.; Keith, T.; Al-Laham, M. A.; Peng, C. Y.; Nanayakkara, A.; Gonzalez, C.; Challacombe, M.; Gill, P. M. W.; Johnson, B. G.; Chen, W.; Wong, M. W.; Andres, J. L.; Head-Gordon, M.; Replogle, E. S.; Pople, J. A. *Gaussian 98*; Gaussian Inc.: Pittsburgh, PA, 1998.

(10) Parr, R. G.; Yang, W. *Density-Functional Theory of Atoms and Molecules*; Oxford University Press: Oxford, U.K., 1989.

(11) (a) Backsay, G. B.; Bytheway, I.; Hush, N. S. *J. Am. Chem. Soc.* **1996**, *118*, 3753. (b) Bytheway, I.; Backsay, G. B.; Hush, N. S. *J. Phys. Chem.* **1996**, *100*, 6023. (c) Maseras, F.; Lledós, A.; Costas, M.; Poblet, J. M. *Organometallics* **1996**, *15*, 2947. (d) Li, J.; Dickson, R. M.; Ziegler, T. *J. Am. Chem. Soc.* **1995**, *117*, 11482. (e) Li, J.; Ziegler, T. *Organometallics* **1996**, *15*, 3844. (f) Camanyes, S.; Maseras, F.; Moreno, M.; Lledós, A.; Lluch, J. M.; Bertrán, J. *J. Am. Chem. Soc.* **1996**, *118*, 4617. (g) Gelabert, R.; Moreno, M.; Lluch, J. M.; Lledós, A. *Organometallics* **1997**, *16*, 3805.

(12) (a) Lee, C.; Yang, W.; Parr, R. G. *Phys. Rev. B* **1988**, *37*, 785. (b) Becke, A. D. *J. Chem. Phys.* **1993**, *98*, 5648.

(13) Hay, P. J.; Wadt, W. R. *J. Chem. Phys.* **1985**, *82*, 299.

(14) Frisch, M. J.; Trucks, G. W.; Schlegel, H. B.; Gill, P. M. W.; Johnson, B. G.; Robb, M. A.; Cheeseman, J. R.; Keith, T. A.; Petersson, G. A.; Montgomery, J. A.; Raghavachari, K.; Al-Laham, M. A.; Zakrzewski, V. G.; Ortiz, J. V.; Foresman, J. B.; Cioslowski, J.; Stefanov, B. B.; Nanayakkara, A.; Challacombe, M.; Peng, C. Y.; Ayala, P. Y.; Chen, W.; Wong, M. W.; Andres, J. L.; Replogle, E. S.; Gomperts, R.; Martin, R. L.; Fox, D. J.; Binkley, J. S.; Defrees, D. J.; Baker, J.; Stewart, J. P.; Head-Gordon, M.; Gonzalez, C.; Pople, J. A. *Gaussian 94*; Gaussian Inc.: Pittsburgh, PA, 1995.

(15) Hehre, W. J.; Ditchfield, R.; Pople, J. A. *J. Chem. Phys.* **1972**, *56*, 2257.

(16) Hariharan, P. C.; Pople, J. A. *Theor. Chim. Acta* **1973**, *28*, 213.

(17) Francl, M. M.; Pietro, W. J.; Hehre, W. J.; Binkley, J. S.; Gordon, M. S.; DeFrees, D. J.; Pople, J. A. *J. Chem. Phys.* **1982**, *77*, 3654.

(18) Gelabert, R.; Moreno, M.; Lluch, J. M.; Lledós, A. *Chem. Phys.* **1999**, *241*, 155.

(19) Tomàs, J.; Lledós, A. *Organometallics* **1998**, *17*, 190.

(20) Peng, C.; Ayala, P. Y.; Schlegel, H. B.; Frisch, M. J. *J. Comput. Chem.* **1996**, *17*, 49.

(21) Light, J. C.; Hamilton, I. P.; Lill, J. V. *J. Chem. Phys.* **1985**, *82*, 1400.

(22) Colbert, D. T.; Miller, W. H. *J. Chem. Phys.* **1992**, *96*, 1982.

(23) Hehre, W. J.; Radom, L.; Schleyer, P. v. R.; Pople, J. A. *Ab Initio Molecular Orbital Theory*; Wiley: New York. 1986.

(24) Scott, A. P.; Radom, L. *J. Phys. Chem.* **1996**, *100*, 16502.

(25) Press, W. H.; Teukolsky, S. A.; Vetterling, W. T.; Flannery, B. P. *Numerical Recipes in FORTRAN*, 2nd ed.; Cambridge University Press: 1992.

Equilibrium Isotope Effect for the $W(CO)_3(PCy_3)_2(H)_2/W(Co)_3(PCy_3)_2(\eta^2\text{-}H_2)$ Tautomeric Equilibrium: A Nuclear Dynamics Variable Representation Study

Laia Torres, Miquel Moreno, and José M. Lluch*

Departament de Química, Universitat Autònoma de Barcelona, 08193 Bellaterra (Barcelona), Spain

Received: October 6, 2000; In Final Form: December 6, 2000

Experimental determination of the equilibrium isotope effect for the dihydride/dihydrogen tautomerism (EIE_T) in the Kubas complex $W(CO)_3(PCy_3)_2(\eta^2\text{-}H_2)$ has not yet been achieved because of the lack of vibrational frequencies for the dihydride form. Even so, Bender, Kubas, Hoff, and co-workers[3] have estimated a normal EIE_T, which predicts that deuterium favors the classical site at 300 K. In this work, EIE_T for the Kubas complex tautomerism is theoretically studied by using two levels of calculation. First, the standard harmonic oscilator approach is used to obtain the harmonic partition functions and the corresponding harmonic EIE_T, which turns out to be inverse (0.485 at 300 K). Next, anharmonicity is included in some normal modes in order to obtain an improved EIE_T. Following a new scheme developed by our group in a previous work,[5] DVR nuclear calculations over bidimensional potential energy surfaces are employed to obtain the associated anharmonic partition functions and the corresponding anharmonic EIE_T, which turns out to be also inverse (0.534 at 300 K). So, theoretical corrected EIE_T predicts that deuterium favors the nonclassical site at 300 K.

Introduction

Due to its important role in catalytic hydrogenation processes, the coordination of H_2 to a transition metal has been one of the most studied phenomena in the recent organometallic chemistry.[1] Depending on the nature of this interaction, two basic types of compounds have been found: those where molecular H_2 coordinates as a two-electron ligand (nonclassical dihydrogen complexes) and those where the H−H bond has been broken to give two one-electron ligands (classical dihydride complexes). Dihydrogen complexes are often thought as intermediates of an oxidative addition of the H_2 to the metal , but today it is accepted that in certain cases a tautomeric equilibrium can exist between the dihydride and the dihydrogen forms (see Scheme 1).

Equilibrium isotope effects (EIE's) for that tautomerism (eq 1) have been reported,[2] but the conclusions diverge to such an extent that, at the moment, no general rule exists concerning whether deuterium favors the classical versus the nonclassical site. Determination of more EIE's would help to understand this reaction, but experimental results in this field are not easy to obtain and, as a consequence, only relatively limited thermodynamic data are available. This is the case for one of the Kubas complexes (the first isolated dihydrogen complexes), whose EIE for the tautomerism has not been strictly resolved because of the lack of experimental data.

(1)

Bender, Kubas, Hoff, and co-workers (BKH) have recently studied[3] the EIE on H_2 binding in the dihydrogen complex $W(CO)_3(PCy_3)_2(\eta^2\text{-}H_2)$. In that work the measured vibrational frequencies arising from the corresponding infrared spectra are used to obtain partition function ratios as described in the general treatment of equilibrium isotope effects by Bigeleisen and Goeppert-Mayer.[4] Once they have the EIE for the H_2 binding

SCHEME 1

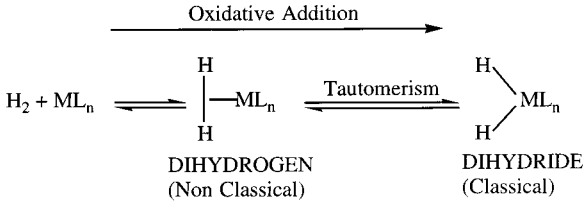

in the Kubas complex, they also try to determine the EIE for eq 1 (EIE_T). It can be defined as the quotient between the EIE for the H_2 binding in the dihydrogen form and the EIE for the H_2 binding in the dihydride form. Determining a generic EIE_T is quite ambitious if we remind that, up to now, no regular behavior has been found among all the studied complexes. To overcome this impasse, BKH employ a particular strategy which consists of assuming that the EIE for the addition of H_2 to the Vaska's complex $Ir(CO)Cl(Ph_3)_2$ (0.46 at 300 K) is typical for the $(H)_2ML_n$ case and that the EIE for Kubas complex $W(CO)_3(PCy_3)_2(\eta^2\text{-}H_2)$ (0.78 at 300 K) is typical for the $(H_2)ML_n$ case. This allow them to estimate the EIE in eq 1, $EIE_T = EIE(2)/EIE(4)$, and hence to predict in general a normal EIE_T—i.e., that deuterium favors the classical site at 300 K. Finally, they try to test the so predicted EIE_T for the $W(CO)_3(PCy_3)_2(\eta^2\text{-}H_2)$ tautomeric equilibrium, but such a validation cannot be achieved because no vibrational frequencies for the dihydride form are available.

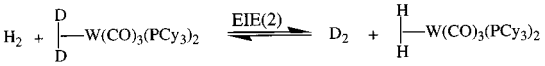

(2)

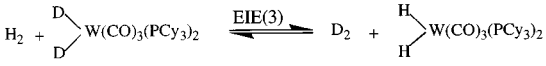

(3)

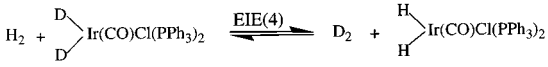

(4)

10.1021/jp0036745 CCC: $20.00
Published on Web 04/19/2001

Starting from this point, our aim is to contribute to the understanding of the dihydride/dihydrogen tautomerism in the Kubas complex $W(CO)_3(PCy_3)_2(\eta^2\text{-}H_2)$ by theoretically obtaining the EIE_T, strictly defined as EIE(2)/EIE(3). In a first step we will calculate it within the harmonic approximation. After that, we will try to improve the results by being more rigorous. In a previous work[5] of our group we concluded that anharmonicity has to be taken into account in order to reproduce and theoretically predict the experimental results concerning many properties of dihydrogen and, probably, polyhydride complexes especially in what refers to isotope effects. Then, in a second step, we will include anharmonicity to correct some normal modes in order to obtain a more accurate EIE_T. This anharmonicity will be introduced by a new scheme derived from quantum nuclear calculations which has been already successfully applied to several dihydrogen complexes.[5]

Calculational Details

In this section we will present the scheme followed to obtain the results of this study. At the same time, we will establish the working conditions, that is, the models that have been assumed, the methods that have been required, and the information that has been borrowed from previous works. The whole process can be divided in two steps: electronic structure calculations; nuclear motion calculations. Both sets of computations are detailed here.

A. Electronic Structure Calculations. In a first step, electronic structure calculations have been done to find the geometry of the minimum energy structures, to compute its molecular partition functions from the harmonic frequencies, and to build up a sizable part of the potential energy surfaces (PES). To save computational effort, the complex under study has been modeled by turning the three cyclohexyl groups into three hydrogen atoms.

All electronic structure calculations have been carried out with the GAUSSIAN 98 series of programs.[6] To solve the electronic Schrödinger equation, the density-functional theory[7] (DFT) methodology has been used. This methodology meets the requirements of high accuracy and reasonable cost and has been employed with great success in the study of several organometallic systems, including dihydrogen and polyhydride complexes.[8,9] The three-parameter hybrid functional of Becke and the Lee, Yang, and Parr correlation functional, widely known as Becke3LYP,[10] has been used. Geometry optimizations have been performed using the Schlegel gradient optimization algorithm using redundant internal coordinates.[11,12]

To reduce the cost of the computations an effective core operator has been used to replace the 60 innermost electrons of the tungsten atom. For the 14 outer electrons of the metal atom the basis set was that associated with the pseudopotential of Hay and Wadt[13] with a standard valence double-ξ LANL2DZ contraction.[11] The basis set for the hydrogen atoms directly attached to the metal was a double-ξ supplemented with a polarization p shell.[14,15] A 6-31G basis set[14] was used for the H atoms attached to a P or a C atom, as well as for carbon and oxygen atoms. The phosphorus atoms were described with the 6-31G(d) basis set.[16]

For each minimum energy structure analytical second derivatives of the energy with respect to the Cartesian coordinates have been computed to obtain the frequencies and eigenvectors associated with each vibrational normal mode within the harmonic approximation. For complexes described by means of pseudopotentials this is a new feature included in GAUSSIAN 98.[6] In this thermochemical calculation, molecular partition functions have also been obtained at 1 atm and 300 K within the ideal gas, rigid rotor, and harmonic oscillator models.

For the dihydrogen form of the studied complex, the minimum energy structure and the harmonic molecular partition functions for the two isotopic versions (H/D) have been taken from a previous paper of our group.[5] For the dihydride form, the geometry for the minimum energy structure has been taken from the authors of ref 17, but all the other magnitudes have been calculated in this work. That dihydride structure accounts[17] for both the spectroscopic and the thermodynamic experimental data.

B. Nuclear Motion Calculations. In this second step, nuclear motion calculations have been carried out to determine vibrational (anharmonic) energy levels and their associated (anharmonic) molecular partition functions.

Anharmonic vibrational energy levels arise from the solution (eigenvalues) of the nuclear Schrödinger equation over a suitable PES built up from electronic calculations. Hence, previously to the nuclear motion study, an adequate PES is required for each minimum energy structure. For the dihydrogen complex, a two-dimensional PES as a function of the interatomic distance between the two hydrogen (deuterium) atoms of the H_2 (D_2) unit of the complex and the distance between the metal atom and the point halfway between those two hydrogen (deuterium) atoms has been taken from our previous work.[5] For the dihydride complex a two-dimensional PES as a function of the interatomic distance between the metal atom and one of the H(D) atoms and the interatomic distance between the metal atom and the other H(D) atom has been constructed. It has to be noted that the two PES coordinates are different from those of the dihydrogen form. This is because the molecular symmetry between the two complexes is different (the criterion we have used to choose these new coordinates is explained in the next section). When the PES is calculated, global relaxation of the rest of geometrical parameters has been allowed.

These two interatomic distances behave as orthogonal coordinates, in such a way that no coupled terms between them appear in the nuclear kinetic operator of the corresponding nuclear Schrödinger equation; that is,

$$\hat{T} = \frac{-\hbar^2}{2\mu_x}\frac{\partial^2}{\partial x^2} + \frac{-\hbar^2}{2\mu_y}\frac{\partial^2}{\partial y^2} \tag{5}$$

where x and y stand respectively for the H−H and $W-H_2$ distances in the dihydrogen complex and $W-H_A$ and $W-H_B$ distances in the dihydride complex.

To solve the nuclear Schrödinger equation the generic discrete variable representation (DVR) proposed by Colbert and Miller[18] has been used. This method has already been applied with success in the field of organometallic chemistry.[8,19] Computationally, the DVR has great advantages over the more traditional variational basis representation, in which the energy levels are obtained by diagonalization of the matrix representation of the projection of the Hamiltonian operator on a given basis set. In short, the DVR is a grid-point representation instead of a basis set representation, and thus, it facilitates the calculation of the potential energy integrals V_{ij}. In this representation, the potential energy matrix is diagonal,

$$V_{ii'} = \delta_{ii'}V(x_i) \tag{6}$$

and the kinetic energy matrix is very simple,

$$T_{ii'} = \frac{\hbar^2(-1)^{i-i'}}{2\mu_x \Delta x^2} \begin{cases} \pi^2/3 & i = i' \\ \dfrac{2}{(i-i')^2} & i \neq i' \end{cases} \tag{7}$$

leading to a very sparse Hamiltonian matrix easier to diagonalize than those coming from a basis set representation,

$$H_{ij,i'j'} = T_{ii'}\delta_{jj'} + T_{jj'}\delta_{ii'} + \delta_{ii'}\delta_{jj'}V(x_i, y_j) \tag{8}$$

Once the grid-point representation of the nuclear Hamiltonian has been built up and diagonalized, the nuclear energy levels obtained have been used to calculate the associated two-dimensional anharmonic vibrational partition function as

$$Q_{\text{anh}} = \sum_j e^{-Ej/k_B T} \tag{9}$$

where k_B is Boltzmann's constant and the summatory extends over all the significantly populated vibrational levels of the 2-D PES.

The total vibrational partition function is then calculated by assuming an independent normal mode framework for the rest of the degrees of freedom (i.e. no mode−mode coupling). In this case the vibrational partition function is the product of Q_{anh} with the individual partition functions corresponding to each additional normal mode. To obtain these individual partition functions, one-dimensional PES should be built up as a function of each normal mode. Our transition-metal complex has 17 nuclei, which implies dealing with 45 vibrtional modes. Application of this procedure to each normal mode is a task out of reach. To simplify the calculations we have assumed that all the modes except the ones included in Q_{anh} behave as harmonic oscillators. This assumption is reasonable if most of the anharmonic correction comes from the two modes chosen to define the 2-D PES and, in any case, provides a first approximation to the total anharmonic vibrational partition function of the molecule.

Results and Discussion

In this section we will present the results obtained from the electronic and nuclear calculations. As we outlined in the Introduction, the discussion will be centered on the understanding of the EIE and it will be presented as follows: In a first step, we will consider the harmonic EIE obtained by the standard approach, and in a second step, we will analyze the anharmonic EIE obtained by following our new procedure.

According to the well-known formulas of the statistical thermodinamics,[20] the deuterium equilibrium isotope effect has been calculated as the equilibrium constant of the equilibrium displayed in eq 1. This equilibrium can also be described as eq 2/eq 3, and hence, the EIE_T has been obtained and presented as EIE(2)/EIE(3), that is, as the quotient between EIE for the dihydrogen formation and the EIE for the dihydride formation.

A. Harmonic EIE. First of all, within the harmonic approximation, we have used the molecular partition functions provided by GAUSSIAN 98 for each chemical species in Figure 1 to evaluate the harmonic EIE's. In addition, we have decomposed each EIE as the product of three factors: the translational−rotational contribution (TRANSROT); the factor corresponding to the contribution of the ground vibrational states, that is, only including the zero-point energy levels (ZPE); the factor that appears when the excited vibrational energy levels are taken into account (EXC). The corresponding results are shown in Table 1.

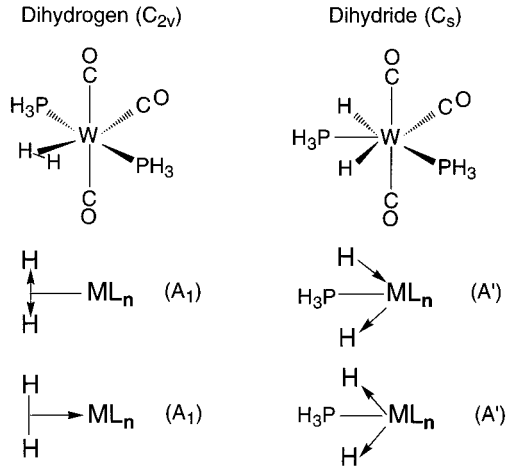

Figure 1. Relevant symmetry coordinates associated with the dihydrogen and the dihydride complexes.

The DFT-calculated harmonic EIE for the dihydrogen formation turns out to be inverse, although numerically is somewhat lesser (that is to say, the isotope effect turns out to be more intense) than the value calculated by BKH[3] from the infrared spectra. The difference stems fundamentally from the ZPE factor, which is the main responsible of the inverse behavior, but that variation is not large enough to be considered a qualitative disaccord. On the other hand, the dihydride formation hardly gives harmonic isotope effect. This is a little surprising if we think that the dihydride complex is almost the same molecule as the dihydrogen one. What has changed? The reason seems to reside on a structural alteration. The dihydrogen structure has a C_{2v} geometry. In turn, the dihydride structure can be described as a pentagonal-bipyramidal C_s complex with axial carbonyls and the two hydrides lying in the equatorial plane being separated by a phosphine ligand[17] (see Figure 1). The P−W−P angle (136.6°) seems large enough to accommodate encumbered phosphines such as PCy_3. In that structure, the two H's cannot be considered as a H_2 unity, and hence, the H−H stretching as such is not a symmetry coordinate contributing to a normal mode anymore. Another result of that coordination change is that the hydrogen motion appears to be more spread out among the normal modes. It participates in a larger number of normal modes, and furthermore, it is more coupled with the motion of the rest of the atoms of the molecule. As a consequence, the relative contribution of the H motion in the dihydride vibrations is less than in the dihydrogen vibrations, and therefore, the normal modes are, in general, less sensitive to the isotopic substitution. That is, the EIE is less important.

Finally, we obtain an inverse EIE_T (EIE for the tautomerism) that differs from the normal EIE predicted by BKH[3], at least within the harmonic approximation. This is not an inconsistency if we bear in mind that they estimate EIE_T as EIE(2)/EIE(4), that is, mixing two different complexes: $W(CO)_3(PCy_3)_2(\eta^2\text{-}H_2)$ as a typical dihydrogen and $(H)_2Ir(CO)Cl(PPh_3)_2$ as a typical dihydride.

B. Anharmonic EIE. As we have previously seen, the first thing we need to do to be able to calculate the anharmonic EIE is to choose which normal modes are to be corrected. A priori, it is not possible to know with certainty which are the most anharmonic normal modes in a molecule, but if we focus on the normal modes which can influence the EIE, we obviously have to consider those associated with the dihydrogen or dihydride ligand.

In the dihydrogen complex the major anharmonicity effect is probably related to the H−H stretching. This motion and the

TABLE 1: Harmonic EIE's and Contributions to Them[a]

	eq 2 $H_2 + (D_2)-WL_n \rightleftharpoons D_2 + (H_2)-WL_n$	eq 3 $H_2 + (D)_2\text{–}WL_n \rightleftharpoons D_2 + (H)_2\text{–}WL_n$	eq 1 $(D_2)-WL_n + (H)_2\text{–}WL_n \rightleftharpoons (H_2)\text{-}WL_n + (D)_2WL_n$
TRANSROT	5.519 (5.77)	5.543	0.996
ZPE	0.131 (0.20)	0.254	0.514
EXC	0.675 (0.67)	0.712	0.948
EIE	0.486 (0.78)	1.002	0.485

[a] Numbers in parentheses correspond to the values calculated by Bender, Kubas, Hoff, and co-workers[3] from the infrared spectra.

$W-H_2$ stretching are the two A_1 symmetry coordinates associated with the dihydrogen ligand[5] and are pictured in Figure 1. Then, the A_1 normal modes derived from these symmetry coordinates have to be considered as anharmonic modes in the sense defined above. In addition, since that anharmonicity couples significantly the two modes of the same symmertry, the independent normal mode framework has been assumed neglecting all the mode−mode couplings but the coupling between the two A_1 modes that has not been separated. On the other hand, in the dihydride complex the reorganization of the ligands leads to a loss of symmetry and, hence, to a change in the normal modes. Since there is a phosphine between, the two H's behave as independent ligands and not as a H_2-bound molecule. For that reason H−H stretching is not a representative component of the normal modes in the dihydride complex, and consequently, it has not been used as a symmetry coordinate. Among the normal modes that include the motion of the two hydrogen atoms, those where heavy atom motions are negligible have been chosen as the anharmonic modes to be corrected (Figure 1) and, as in the dihydrogen case, not to be separated by the independent normal mode framework. In both dihydrogen and dihydride cases, the two normal modes chosen have been studied together over a two-dimensional PES.

The two-dimensional PES for the dihydrogen complex was already presented in a previous paper as a function of the two symmetry coordinates.[5] A collection of 120 electronic structure calculations, each corresponding to a different set of H−H and $W-H_2$ distances, covered ranges from 0.6 to 2.0 Å for the H−H distance and from 1.4 to 2.5 Å for the $W-H_2$ distance. The resulting points were fitted into a two-dimensional cubic splines functional form,[21] which is a smooth and continuous function. Figure 2 depicts the two-dimensional PES as a contour plot.[5] For the dihydride complex a two-dimensional PES has been built up by calculating 56 points, each one corresponding to a different set of $W-H_A$ and $W-H_B$ distances, covering ranges from 1.5 to 2.2 Å for the $W-H_A$ distance and from 1.5 to 2.1 Å for the $W-H_B$ distance. These 56 points are necessary to cover the PES until an energy of at least 10 kcal/mol above the minimum is reached. Since the two hydride ligands are not equivalent, the extent of the $W-H_A$ distance and the $W-H_B$ distance is not exactly the same. It has to be noted that, in this case, the symmetry coordinates used to represent the anharmonic normal modes do not coincide with the axes of the bidimensional PES but with its two diagonals. It has been necessary to expand this PES made of electronic structure calculations. The reason is that DVR results are sometimes difficult to converge due to the fictitious energy gap present at the edge of the PES (the method works as if there were an infinite potential wall at the border). To save computational effort, this enlargement has been done by using a two-dimensional analytic harmonic potential that generates the harmonic frequencies of the two corrected normal modes. The anharmonicity which can affect the EIE is that of the region next to the minimum. Therefore, the use of this supplementary harmonic potential is not incompatible with the introduction of anharmonicity. Figure 3 depicts the resulting two-dimensional PES as a contour plot.

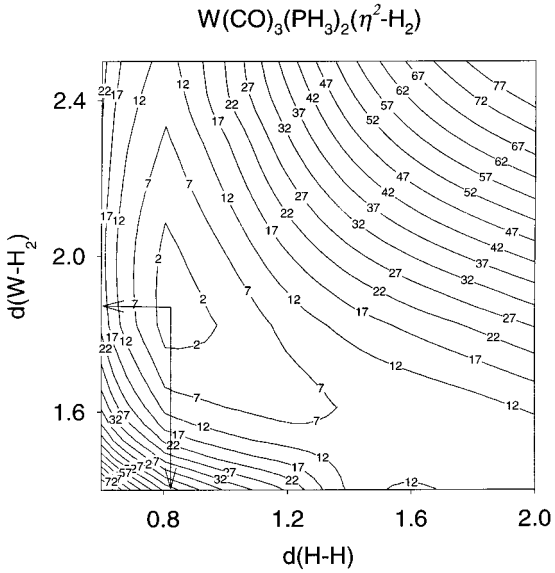

Figure 2. Contour plot of the two-dimensional potential energy surface for the dihydrogen complex $W(CO)_3(PH_3)_2(\eta^2\text{-}H_2)$. Distances are given in Å. Energy contours appear every 5 kcal/mol. The arrows indicate the position of the minimum energy structure (d(H−H) = 0.832 Å and $d(W-H_2)$ = 1.872 Å).

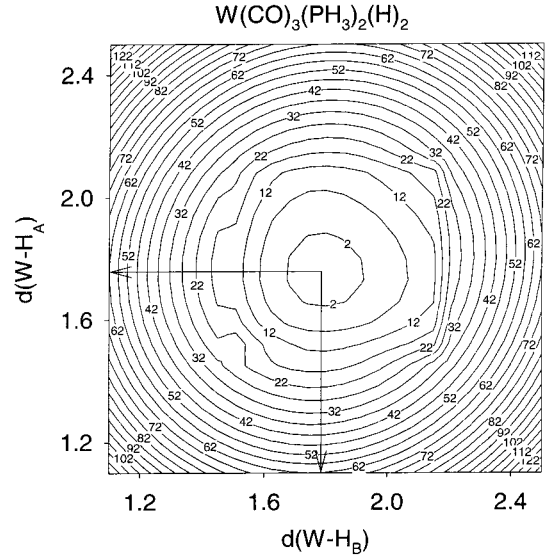

Figure 3. Contour plot of the two-dimensional potential energy surface for the dihydride complex $W(CO)_3(PH_3)_2(H)_2$. Distances are given in Å. Energy contours appear every 10 kcal/mol. The arrows indicate the position of the minimum energy structure ($d(W-H_A)$ = 1.788 Å and $d(W-H_B)$ = 1.753 Å).

Comparison between Figures 2 and 3 discloses some remarkable differences regarding the shape of the two PES in the region of the minima. The dihydride complex presents a typical harmonic pattern with the two normal modes, symmetric and antisymmetric H_A-M-H_B stretching, being the sum and the subtraction of the two W−H distances respectively (that is, the

TABLE 2: Anharmonic EIE's (See Text) and Contributions to Them[a]

	eq 2 $H_2 + (D_2)-WL_n \rightleftharpoons D_2 + (H_2)-WL_n$	eq 3 $H_2 + (D)_2\text{–}WL_n \rightleftharpoons D_2 + (H)_2\text{–}WL_n$	eq 1 $(D_2)-WL_n + (H)_2\text{–}WL_n \rightleftharpoons (H_2)\text{-}WL_n + (D)_2WL_n$
TRANSROT	5.519 (5.77)	5.543	0.996
ZPE	0.143 (0.20)	0.254	0.563
EXC	0.676 (0.67)	0.710	0.952
EIE	0.534 (0.78)	1.001	0.534

[a] Numbers in parentheses correspond to the values calculated by Bender, Kubas, Hoff, and co-workers[3] from the infrared spectra.

two diagonals of the PES in Figure 3). In view of this shape, we can expect that the introduction of anharmonicity will not change significantly the EIE results. Conversely, the potential energy valley for the dihydrogen complex is almost parallel to the $W-H_2$ axis with a trend to curve along the H−H direction as the $W-H_2$ distance shortens (Figure 2). As a consequence, the two normal modes of A_1 symmetry, although mixed to some extent (as already pointed out by BKH[3]), can still be identified respectively with the two A_1 symmetry coordinates. That is to say, one normal mode is basically the H−H stretching and the other one is essentially the symmetric $M-H_2$ stretching. Unlike the dihydride, this energy valley shows some anharmonic character, and hence, in this case we can expect that the introduction of anharmonicity do will change the EIE results.

Once the potential energy surfaces have been obtained, the corresponding nuclear Schrödinger equations can be solved using the DVR method. Prior to that, a certain reduced mass has to be assigned to each degree of freedom in the Hamiltonian. As in our previous works,[7,22] the reduced masses for the motion along the coordinates have been calculated (for the perprotio complexes) as

$$\frac{1}{\mu_{d(H-H)}} = \frac{1}{m_{H_A}} + \frac{1}{m_{H_B}}$$

$$\frac{1}{\mu_{d(M-H_2)}} = \frac{1}{m_{H_2}} + \frac{1}{m_{[ML_n]}} \qquad (10)$$

for the dihydrogen complex and

$$\frac{1}{\mu_{d(M-H_A)}} = \frac{1}{m_{H_A}} + \frac{1}{m_{[ML_nH_B]}}$$

$$\frac{1}{\mu_{d(M-H_B)}} = \frac{1}{m_{H_B}} + \frac{1}{m_{[ML_nH_A]}} \qquad (11)$$

for the dihydride complex. Note that the reduced masses of the dideuterated complexes can be calculated in an analogous way. Then, the matrix representation of the nuclear Hamiltonian over a rectangular grid of equally spaced points has been constructed. Different sizes of each grid have been tested until convergence of the energy levels has been achieved. The characteristics of the final grids chosen for the different systems have been as follows: $35 \times 27 = 945$ for both the perprotio and the dideuterated dihydrogen complexes and $35 \times 35 = 1225$ for both the perprotio and the dideuterated dihydride complexes (the format used is the following: number of points along the *x* coordinate × number of points along the *y* coordinate = total number of points). Diagonalization of the corresponding matrixes provides the sets of vibrational wave functions (eigenvectors) and anharmonic energy levels (eigenvalues). These energy levels permit the calculation of the anharmonic vibrational partition function of each molecule according to the procedure outlined in the previous section so that the anharmonic EIE's are obtained. The corresponding anharmonic EIE's are shown in Table 2.

Table 2 exhibits the anharmonic EIE's and their decomposition in factors (evidently the TRANSROT contribution is the same as in Table 1). Comparison of Tables 1 and 2 shows that anharmonicity does not significantly alter the EXC factor. The important changes only concern the ZPE factor. For the dihydride, no changes appear in the anharmonic EIE(3), which means that the harmonic approximation is valid to study the thermochemistry of this complex. For the dihydrogen complex, instead, anharmonicity augments slightly the ZPE contribution and, therefore, the EIE(2). The anharmonic EIE(2), still clearly inverse, is somewhat closer to the experimental values than the harmonic EIE(2). If one takes into account the range of uncertainty of the experimental values[3] (0.78 from infrared spectra or 0.70 ± 0.15 from displacement of N_2) and that anharmonicity has been only partially incorporated, the agreement is rather good. As we saw in our previous work, anharmonicity tends to favor the addition of H_2 because it weakens the lowering of the vibrational energy levels due to the isotopic substitution. The larger the anharmonicity of the normal modes sensitive to the isotopic substitution in the dihydrogen complex, the smaller the gap between the equivalent HH and DD vibrational energy levels. Along the addition in eq 2, the change in the HH/DD zero-point energy gap for the normal mode corresponding originally to the H−H (D−D) stretching in the free hydrogen molecule gives a normal ZPE factor (a value greater than unity). On the contrary, conversion of the 5 translational and rotational modes in free hydrogen to vibrational normal modes in the dihydrogen complex leads to an inverse ZPE factor (a value smaller than unity). As a consequence of all this, anharmonicity increases the numerical value of the ZPE factor associated with the dihydrogen ligand (the normal and inverse factors become more normal and less inverse, respectively), so tending to produce a normal EIE.

The anharmonicity of the dihydrogen complex is reflected in the anharmonic EIE_T for the tautomerism. As in the harmonic results, anharmonic EIE_T turns out to be inverse, although in a less extent.

Conclusions

In this work we have theoretically studied the equilibrium isotope effect for the dihydride/dihydrogen tautomerism (EIE_T) in the Kubas complex $W(CO)_3(PCy_3)_2(\eta^2\text{-}H_2)$. Experimental determination of this magnitude has not been achieved due to the lack of vibrational frequencies for the dihydride form. There is only an estimation by Bender, Kubas, Hoff, and co-workers[3] that predicts a normal EIE_T, that is, that deuterium favors the classical site at 300 K.

We have first calculated the harmonic EIE_T arising from the standard thermodynamic analysis (within the ideal gas, rigid rotor, and harmonic oscilator models). Prior to that it has been necessary to characterize the geometry of the minimum energy structures and to compute its molecular partition functions. These electronic DFT calculations have given an inverse $EIE_T = 0.485$ at 300 K. In view of the difference from the predicted normal behavior, a deeper treatment has been done in order to

obtain a more accurated EIE_T. Beyond the harmonic approach, nuclear calculations over bidimensional potential energy surfaces have been performed. Particularly, DVR methodology has been used to obtain the corresponding vibrational energy levels of each structure, and finally, following a new scheme developed by our group in a previous work,[5] anharmonic partition functions have been obtained and used to compute the corrected EIE_T. These nuclear calculations have given again an inverse $EIE_T = 0.534$ at 300 K. Therefore, although being less inverse than the harmonic result, the anharmonic EIE_T also indicates that deuterium favors the nonclassical site at 300 K. This result contrasts with the small normal kinetic isotope effect (KIE) for conversion of the dihydride to the dihydrogen tautomers measured by Hoff and co-workers.[23] However, it has to be realized that the KIE (a kinetic magnitude) and its corresponding EIE (a thermodynamic magnitude) can behave in a different way.

The conclusion outlined above for the Kubas complex is not a general rule which can be applied to any dihydride/dihydrogen tautomerism. The EIE_T has been rigorously calculated here only for the Kubas complex. Actually, several experimental EIE_T's have been reported[2] and conclusions diverge from one complex to another. It seems that this is such an intricate chemical process that no direct extrapolation would be valid to make predictions for whatever dihydride/dihydrogen tautomerism at whatever temperature. With the aim of understanding the dihydride/dihydrogen tautomerism, additional experimental and theoretical studies would be necessary. Work on this topic is now in progress in our laboratory.

Acknowledgment. Financial support from the DGESIC through Project PB98-0915 and the use of the computational facilities of the CESCA and CEPBA coordinated by the C[4] are gratefully acknowledged.

References and Notes

(1) Heinekey, D. M.; Oldham, W. J., Jr. *Chem. Rev.* **1993**, *93*, 913.

(2) (a) Luo, X.-L.; Crabtree, R. H. *J. Am. Chem. Soc.* **1990**, *112*, 6912. (b) Haward, M. T.; George, M. W.; Hamley, P.; Poliakoff, M. *J. Chem. Soc., Chem. Commun.* **1991**, 1101. (c) Gusev, D. G.; Nietlispach, D.; Eremenko, I. L.; Berke, H. *Inorg. Chem.* **1993**, *32*, 3628. (d) Henderson, R. A.; Oglieve, K. E. *J. Chem. Soc., Dalton. Trans.* **1993**, 3431. (e) Heinekey, D. M.; Oldham, W. J., Jr. *J. Am. Chem. Soc.* **1994**, *116*, 3137.

(3) Bender, B. R.; Kubas, G. J.; Jones, L. H.; Swanson, B. I.; Eckert, J.; Capps, K. B.; Hoff, C. D. *J. Am. Chem. Soc.* **1997**, *119*, 9179.

(4) Bigeleisen, J.; Goeppert-Mayer, M. *J. Chem. Phys.* **1947**, *15*, 261.

(5) Torres, L.; Gelabert, R.; Moreno, M.; Lluch, J. M. *J. Phys. Chem. A* **2000**, *104*, 7898.

(6) Frisch, M. J.; Trucks, G. W.; Schlegel, H. B.; Scuseria, G. E.; Robb, M. A.; Cheeseman, J. R.; Zakrzewski, V. G.; Montgomery, J. A.; Stratmann, R. E.; Burant, J. C.; Dapprich, S.; Millam, J. M.; Daniels, A. D.; Kudin, K. N.; Strain, M. C.; Farkas, O.; Tomasi, J.; Barone, V.; Cossi, M.; Cammi, R.; Mennucci, B.; Pomelli, C.; Adamo, C.; Clifford, S.; Ochterski, J.; Petersson, G. A.; Ayala, P. Y.; Cui, Q.; Morokuma, K.; Malick, D. K.; Rabuck, A. D.; Raghavachari, K.; Foresman, J. B.; Cioslowski, J.; Ortiz, J. V.; Stefanov, B. B.; Liu, G.; Liashenko, A.; Piskorz, P.; Kamaromi, I.; Gomperts, R.; Martin, R. L.; Fox, D. J.; Keith, T.; Al-Laham, M. A.; Peng, C. Y.; Nanayakkara, A.; Gonzalez, C.; Challacombe, M.; Gill, P. M. W.; Johnson, B. G.; Chen, W.; Wong, M. W.; Andres, J. L.; Head-Gordon, M.; Replogle, E. S.; Pople, J. A. *Gaussian 98*; Gaussian Inc.: Pittsburgh, PA, 1998.

(7) Parr, R. G.; Yang, W. *Density-Functional Theory of Atoms and Molecules*; Oxford University Press: Oxford, U.K., 1989.

(8) (a) Gelabert, R.; Moreno, M.; Lluch, J. M.; Lledós, A. *J. Am. Chem. Soc.* **1997**, *119*, 9840. (b) Gelabert, R.; Moreno, M.; Lluch, J. M.; Lledós, A. *J. Am. Chem. Soc.* **1998**, *120*, 8168.

(9) (a) Backsay, G. B.; Bytheway, I.; Hush, N. S. *J. Am. Chem. Soc.* **1996**, *118*, 3753. (b) Bytheway, I.; Backsay, G. B.; Hush, N. S. *J. Phys. Chem.* **1996**, *100*, 6023. (c) Maseras, F.; Lledós, A.; Costas, M.; Poblet, J. M. *Organometallics* **1996**, *15*, 2947. (d) Li, J.; Dickson, R. M.; Ziegler, T. *J. Am. Chem. Soc.* **1995**, *117*, 11482. (e) Li, J.; Ziegler, T. *Organometallics* **1996**, *15*, 3844. (f) Camanyes, S.; Maseras, F.; Moreno, M.; Lledós, A.; Lluch, J. M.; Bertrán, J. *J. Am. Chem. Soc.* **1996**, *118*, 4617. (g) Gelabert, R.; Moreno, M.; Lluch, J. M.; Lledós, A. *Organometallics* **1997**, *16*, 3805.

(10) (a) Lee, C.; Yang, W.; Parr, R. G. *Phys. Rev. B* **1988**, *37*, 785. (b) Becke, A. D. *J. Chem. Phys.* **1993**, *98*, 5648.

(11) Frisch, M. J.; Trucks, G. W.; Schlegel, H. B.; Gill, P. M. W.; Johnson, B. G.; Robb, M. A.; Cheeseman, J. R.; Keith, T. A.; Petersson, G. A.; Montgomery, J. A.; Raghavachari, K.; Al-Laham, M. A.; Zakrzewski, V. G.; Ortiz, J. V.; Foresman, J. B.; Cioslowski, J.; Stefanov, B. B.; Nanayakkara, A.; Challacombe, M.; Peng, C. Y.; Ayala, P. Y.; Chen, W.; Wong, M. W.; Andres, J. L.; Replogle, E. S.; Gomperts, R.; Martin, R. L.; Fox, D. J.; Binkley, J. S.; Defrees, D. J.; Baker, J.; Stewart, J. P.; Head-Gordon, M.; Gonzalez, C.; Pople, J. A. *Gaussian 94*; Gaussian Inc.: Pittsburgh, PA, 1995.

(12) Peng, C.; Ayala, P. Y.; Schlegel, H. B.; Frisch, M. J. *J. Comput. Chem.* **1996**, *17*, 49.

(13) Hay, P. J.; Wadt, W. R. *J. Chem. Phys.* **1985**, *82*, 299.

(14) (a) Hehre, W. J.; Ditchfield, R.; Pople, J. A. *J. Chem. Phys.* **1972**, *56*, 2257. (b) Hariharan, P. C.; Pople, J. A. *Theor. Chim. Acta* **1973**, *28*, 213.

(15) Hariharan, P. C.; Pople, J. A. *Theor. Chim. Acta* **1973**, *28*, 213.

(16) Francl, M. M.; Pietro, W. J.; Hehre, W. J.; Binkley, J. S.; Gordon, M. S.; DeFrees, D. J.; Pople, J. A. *J. Chem. Phys.* **1982**, *77*, 3654.

(17) Tomàs, J.; Lledós, A.; Jean, Y. *Organometallics* **1998**, *17*, 190.

(18) Colbert, D. T.; Miller, W. H. *J. Chem. Phys.* **1992**, *96*, 1982.

(19) McQuarrie, D. A. *Statistical Thermodynamics*; University Science Books: Mill Valley, CA, 1973.

(20) Press: W. H.; Teukolsky, S. A.; Vetterling, W. T.; Flannery, B. P. *Numerical Recipes in FORTRAN*, 2nd ed.; Cambridge University Press: New York, 1992.

(21) (a) Scheurer, C.; Wiedenbruch, R.; Meyer, R.; Ernst, R. R.; Heinekey, D. M. *J. Chem. Phys.* **1996**, *106*, 1. (b) Maseras, F.; Lledós, A.; Clot, E.; Eisenstein, O. *Chem. Rev.* **2000**, *100*, 601.

(22) Gelabert, R.; Moreno, M.; Lluch, J. M.; Lledós, A. *Chem. Phys.* **1999**, *241*, 155.

(23) Zhang, K.; González, A. A.; Hoff. C. D. *J. Am. Chem. Soc.* **1989**, *111*, 3627.

Semiclassical initial value representation description of molecular structure problems: An elongated dihydrogen ruthenium complex

Laia Torres and Ricard Gelabert
Departament de Química, Universitat Autònoma de Barcelona, 08193 Bellaterra (Barcelona), Spain

Xavier Giménez
Departament de Química Física, Universitat de Barcelona. Martí i Franquès, 1, 08028 Barcelona, Spain and Centre Especial de Recerca en Química Teòrica, Parc Científic de Barcelona. Baldiri Reixach, 10–12, 08028 Barcelona, Spain

Miquel Moreno and José M. Lluch
Departament de Química, Universitat Autònoma de Barcelona, 08193 Bellaterra (Barcelona), Spain

(Received 13 June 2002; accepted 2 July 2002)

The Herman–Kluk initial value representation semiclassical approach has been applied, and proven effective, as well as accurate, to account for the intriguing elongated dihydrogen structure in a ruthenium coordination complex. Results are satisfactory even though the reduced dimensionality two-dimensional potential, involving the relevant distances, casts an extremely anharmonic, weakly bound species, with two exit channels. Comparatively short propagation times, to avoid complications due to chaotic trajectories, as well as discarding trajectories exiting the effective potential energy surface, has proven effective to converge results, as indicated by comparison with quantum mechanical discrete variable representation data. © *2002 American Institute of Physics.* [DOI: 10.1063/1.1502649]

I. INTRODUCTION

The semiclassical (SC) method has recently undergone a rebirth of interest, especially since it was understood that, thanks to several improvements in its formulation, most of its numerical difficulties could be effectively bypassed. Thus, the Herman–Kluk (HK, or coherent state, or minimum uncertainty) version, formulated within the initial value representation (IVR) of the stationary phase (SP) approximation to the time evolution propagator, has been proven as a reliable, numerically efficient technique for dealing with a wealth of molecular problems.[1–5] Its main advantage is the avoidance of the exponential increase in numerical effort, as the number of degrees of freedom increases, typical of quantum mechanical formulations of dynamical problems, whereas, at the same time, it is capable of describing quite accurately, quantum effects. These effects, contrary to previous expectations, are becoming more important as new experiments (with improved time and position resolution power) are available.

Among specific applications, one should mention model condensed phase problems,[6] cumulative reaction probabilities,[7] femtosecond spectroscopy of I_2^-,[8] molecular energy transfer,[9] thermal rate constant calculations,[10] quantum coherence/decoherence in molecular vibrations,[11] as well as diffraction through a double slit potential barrier coupled to a thermal bath.[12,13] These cases, along with several recent improvements in the methodology,[2–5] clearly show that the SC approach is fastly approaching a widespread use in the study of molecular problems.

Two specific difficulties, though, still persist, casting some doubts into the possibility of firmly establishing the SC approach as a routine tool. The first one concerns the highly oscillatory nature of the integrand, which is characteristic of the integral appearing in the SC-IVR approach to the time evolution operator. It arises as a consequence of its complex valued origin. The multidimensional character of the integrand, in addition, forces the use of Monte Carlo sampling techniques to reduce the computational effort. The second difficulty is related to the so-called prefactor since, corresponding to a stability (monodromy) calculation, it is found to take very high values when the motion approaches chaotic regimes. In particular, it can be shown that the simple probing of convex regions in the potential energy surface (PES) suffices to make the prefactor, for long enough time propagations, grow up to troublesome values. Actually, a third difficulty, closely tied to the first, arises in problems where, e.g., a thermal average is necessary. It corresponds to the difficulty of having a proper weighting function in the Monte Carlo integration, thus preventing a straightforward extension of the method to truly complex systems.

An intense methodological effort is being devoted towards solving the above difficulties. Generalized filtering procedures have been proposed to reduce the oscillatory nature of the integrand.[2] In addition, a symmetrized form of flux correlation functions has been recently shown to provide a well-behaved integral in thermalized problems.[5] As for the prefactor behavior, however, a more effective yet accurate formulation looks still elusive,[14] even though some interesting progress has been reported recently for nonchaotic systems.[15] Being a direct consequence of the SP approximation (or, more generally, steepest descent techniques applied to the calculation of complex valued integrands),[16] the prefactor plays a decisive role since its value is related to the overall probability of the process under study.[17] The issue is

that, in present-day applications, one must deal very carefully with it, otherwise meaningless results, or extremely slow convergences, might be obtained.

The above discussion will prove of full relevance when one considers the kind of application dealt with in the present work. It consists of the use of the SC methodology directly to study molecular structure problems, in particular those concerning the equilibrium geometry of the so-called elongated dihydrogen transition metal complexes. The complexes which present hydrogen atoms in the coordination sphere of the metal are currently being classified into two large groups: those in which the distance between hydrogen atoms exceeds 1.6 Å, which have been known for a long time and are referred as classical polyhydrides in the literature, and those in which this same distance has a value between 0.8 and 1.0 Å, first discovered by Kubas and which have been known as ''nonclassical dihydrogen complexes.'' [18] The difference between both types of complexes has faded with time due to the discovery of a series of complexes whose H–H distances fall between the two above mentioned limits.[18(c)] These complexes, known as elongated dihydrogen complexes, have been found both in solution and in solid-state structures.

In principle, one may routinely attack the theoretical geometry prediction of these elongated complexes by means of any of the quantum chemistry packages. The issue is then a matter of choosing an optimal strategy for the (approximated) method of calculation, as well as the electronic basis set. However, the resulting equilibrium geometry, concerning specifically the H–H distance, clearly fails to explain the experimental findings, irrespective of the accuracy in the quantum chemistry calculations. In other words, *ab initio* calculations did show that the corresponding species was stable, but the electronic potential energy minima was found to be at much shorter distances than those correspondingly inferred from neutron diffraction measurements.

A plausible explanation was worked out by Gelabert *et al.*[19] By looking at the considerable anharmonicity of the related bond energy functions, it was argued that the nuclear wave function might possibly peak at distances far from the electronic minimum. Discrete variable representation (DVR) calculations for a two-dimensional (2D) effective potential did show the predicted shifting. In addition, such an effect should be sensitive to population changes in the supported vibrational levels, i.e., the geometry had to be, in a measurable degree, temperature dependent. It was found again a good agreement (at the semiquantitative level) between the experimental data and theoretical Boltzmann-weighted average positions, at different temperatures.

One may thus finally recap the story by reversing the above discussion. Thus, delocalization of hydrogen nuclei, a purely quantum mechanical effect originating in strongly anharmonic bonds, is experimentally detectable in elongated dihydrogen transition metal coordination compounds. It shows up in the form of equilibrium geometries which evidence an important mismatch between the actual experimental values and the electronic potential energy minima.

From the outset, the present problem looked prospectively as a good candidate for being studied under the semiclassical framework. Not only is this the first time, as far as we know, that such a feature has been interpreted semiclassically; this is also a stringent test on the capabilities of the SC-IVR approach. The determination of the equilibrium structure may be performed semiclassically starting from a SC-IVR time propagation. After a sufficiently long time the autocorrelation function of the time evolved wave packet is Fourier transformed so as to extract the energy spectrum, as well as the corresponding stationary vibrational wave functions. An accuracy check is rigorously available in the present case, since the 2D PES permitted a previous DVR eigenvalue–eigenvector quantum mechanical calculation. The extraction of the energy spectrum from time-evolved wave packets has been already used in the past,[20,21] to study the rovibrational spectra of strongly, as well as weakly bounded molecules. Here we extend these studies to a specific molecular structure problem.

Thus, the relevant calculation in the present problem is the wave function amplitude, from which the average position is extracted. This is a well-known problem, so that the issue here is the numerical performance when obtaining it, i.e., are the PES features sufficiently well-behaved to allow for the SC-IVR calculation to converge the position expectation value? Certainly, the weakly bound (~20 kcal/mol) species, along with a rather remarkable anharmonicity of the potential profile (plus the existence of two exiting routes to dissociation/rearrangement), pose serious *a priori* difficulties. On the one hand, the small binding character of the PES together with the two exit channels, make somewhat cumbersome accumulating bounded trajectories, so as to reach a low enough statistical error. One may argue that this should not really be a problem, since the exiting trajectories, being overlapped with the initial wave packet in the SC-IVR calculation, are automatically dropped from contributing to the phase space average. On the other hand, these exiting trajectories, jointly to those probing the highly anharmonic regions of the PES (i.e., trajectories propagated for sufficiently long time), often lead to exceedingly large prefactors that contaminate the calculation and thus ruin the convergence rate.

Therefore, succeeding in the present application dramatically depends on the possibility of reaching a compromise on the number of trajectories needed: it should be large enough to guarantee proper Monte Carlo statistics, but not as large as to make the calculation unfeasible. Besides, a similar situation exists for the propagation time; it should be long enough to improve the resolution of the energy spectrum, but kept as short as possible to avoid prefactor exponential growth associated with chaotic dynamics. Specific results in the present work will show that both compromises are possible, operationally, hence opening the way for applying the IVR-SC approach to this kind of problems.

The remainder of the paper has been organized so that Sec. II describes the PES electronic calculation and briefly summarizes how the HK-SC-IVR approach is applied to the present molecular structure problem. Section III shows and discusses the numerical results, for both the PES and the semiclassical calculations. Finally, Sec. IV concludes.

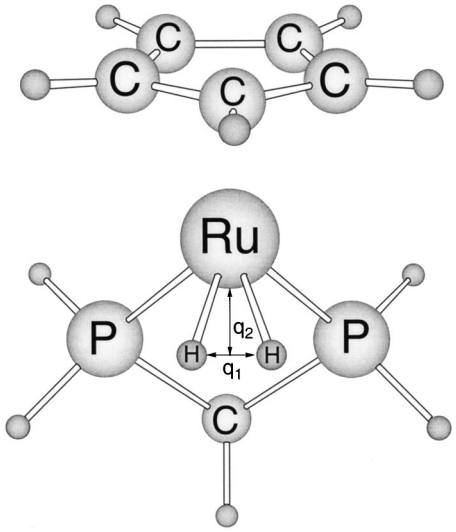

FIG. 1. Optimized structure for the $[Ru(H\cdots H)(C_5H_5)(H_2PCH_2PH_2)]^+$ complex. Arrows show the two parameters q_1 and q_2 chosen as a reduction of the dimensionality of the whole hypersurface.

II. CALCULATION STRATEGY

A. The potential energy surface

The complex under study is the elongated dihydrogen complex $[Ru(H\cdots H)(C_5Me_5)(dppm)]^+$ (dppm = bis(diphenylphosphino)-methane), modeled as $[Ru(H\cdots H)(C_5H_5)(H_2PCH_2PH_2)]^+$ in order to save computational effort. Its structure is shown in Fig. 1. The electronic structure calculations were performed with the GAUSSIAN 94 series of programs,[22] the DFT (Ref. 23) formalism being used throughout, with the three-parameter hybrid functional of Becke and the Lee, Yang, and Parr's correlation functional, widely known as Becke3LYP.[24] This methodology meets the requirements of high accuracy and reasonable cost, and has been employed with great success in the study of several organometallic systems, including dihydrogen and polyhydride complexes.[19,25] An effective core operator was used to replace the inner electrons of the ruthenium atom, in this way eliminating 28 electrons from the system.[26] The basis set associated with the pseudopotential of Hay and Wadt[26] with standard valence double-ζ LANL2DZ contraction,[22] was used for the remaining electrons of the Ru atom. As for the remaining atoms, the standard split-valence 6-31G basis set was chosen,[27] except for (a) the phosphorous atoms, for which the basis set 6-31G(d) was used,[28] and (b) the hydrogen atoms directly bound to the metal, for which the 6-31G(p) basis was considered.[27,29]

B. Application of the SC-HK-IVR approach

The basis of the present application is the time propagation of an initial wave packet, so that it is allowed to probe the characteristic features of the PES. One then goes ahead parallel to the treatments of linear spectroscopy, e.g., performing a Fourier transform of an autocorrelation function involving a single-time propagation,

$$C(t)=\langle\psi_i|e^{-iHt/\hbar}|\psi_i\rangle. \tag{1}$$

It is interesting to note in passing that, involving the calculation of an amplitude, rather than a probability, the integrand in Eq. (1) is complex and contains the important phase information for quantum effects. But, at the same time, its oscillatory character is the main source of the above-mentioned convergence problems.

Within the SC-HK-IVR scheme, the time evolution propagator is given by

$$e^{-iHt/\hbar}=\frac{1}{(2\pi\hbar)^F}\int\int dp_0dq_0C_t(p_0q_0) \times e^{(i/\hbar)S_t(p_0q_0)}|p_tq_t\rangle\langle p_0q_0\rangle, \tag{2}$$

where $F=2$, (p_0q_0) are the initial positions and momenta, (p_tq_t) are the corresponding time-evolved variables, $S_t(p_0q_0)$ is the classical action,

$$S_t(p_0q_0)=\int_0^t dt'[p\dot{q}-H], \tag{3}$$

whereas $|p_tq_t\rangle$ and $\langle p_0q_0|$ are the coherent state, minimum uncertainty wave packets at times t and 0, respectively. Finally, C_t is the Herman–Kluk prefactor, given by

$$C_t^2=2^{-F}\left|M_{qq}+\gamma^{-1}M_{pp}\gamma+\frac{i}{\hbar}\gamma^{-1}M_{pq}+\frac{\hbar}{i}M_{qp}\gamma\right| \tag{4}$$

being $M_{zz'}$ (with $z,z'=p,q$) the elements of the monodromy (stability) matrix

$$M_{zz'}=\frac{\partial z_t}{\partial z_0'}. \tag{5}$$

In expression (4), γ is a constant related to the width of the coherent wave packet. The analytical form for the latter, in the position representation, is

$$\langle q'|pq\rangle=\left(\frac{|\gamma|}{\pi}\right)^{1/4}\exp\left\{-\frac{1}{2}(q'-q)^T\gamma(q'-q) +ip^T(q'-q)\right\}. \tag{6}$$

It is worth noting here that the above formulas become much simpler if one defines γ-scaled coordinates and momenta,

$$q\rightarrow\gamma^{-1/2}q;\quad p\rightarrow\gamma^{1/2}p, \tag{7}$$

since, e.g., the prefactor now becomes

$$C_t^2(z_0)=\left|\frac{1}{2}(1,-i)M\begin{pmatrix}1\\ i\end{pmatrix}\right|. \tag{8}$$

The calculation of the autocorrelation function in Eq. (1) then involves an overlap between two coherent states, which in this compact form avoids the explicit γ-dependence,

$$\langle p_0q_0|p_iq_i\rangle=\exp\left\{-\frac{1}{4}(q_0-q_i)^2-\frac{1}{4}(p_0-p_i)^2 +\frac{i}{2}(p_0+p_i)^T(q_0-q_i)\right\}. \tag{9}$$

The specific implementation on the SC-HK-IVR approach has been performed, in the present work, using the log-derivative version of the HK prefactor, whose derivation has

been presented elsewhere.[12,30] It has the advantage that, when the Gaussian widths are chosen to match one or several of the natural frequencies of the system, the occurrence of branch-cuts in the prefactor calculation is avoided, thus leading to a more efficient integration of the equations of motion, since no tracking of the Maslov index[31] is necessary.

Finally, a standard Fourier transform of the autocorrelation function (1) leads to the desired energy spectrum and associated eigenfunctions, according to the following expressions:

$$I(E)=\frac{1}{\pi\hbar}\mathrm{Re}\int_0^\infty e^{iEt/\hbar}\langle\psi(0)|\psi(t)\rangle e^{-\alpha^2t^2}dt \tag{10}$$

for the energy spectrum, and

$$|\Phi_n\rangle\propto\frac{1}{2T}\int_{-T}^{T}e^{(i/\hbar)E_nt}|\psi(t)\rangle dt \tag{11}$$

for the eigenfunction associated to the nth eigenvalue.[32] In Eq. (10), a Gaussian filtering determined by the α parameter has been applied, so as to obtain noise-free peaks which uniquely identify the true eigenvalues of the potential energy surface.[33]

Before presenting the results of the calculations, it is interesting to explain how the semiclassical parameters, i.e., widths of the coherent state of the Herman–Kluk propagator, propagation time length, number of times the wave packet had to be computed during the propagation, as well as the total number of trajectories, were determined.

The initial total energy of a trajectory is crucial in the present study: if too high, the trajectory will probably escape from the PES. An escaped trajectory is not representative of the behavior of the system because it runs out from the PES, so that it does not describe the bounded motion characteristic of a stable chemical species. Furthermore, the weak bonding character of the PES tells that having an excess of initial energy will quite likely occur. Therefore, we had to tune the wave packet width so as to minimize the total energy of the initial wave packet, in order to have as few runaway trajectories as possible. After the corresponding calibration, the chosen values for the widths of the coherent state of the Herman–Kluk propagator were $\gamma_{q1}=0.009$ and $\gamma_{q2}=0.008$ Å^{-2} uma^{-1}.

The time length of the propagation is also very critical. If too short, the eigenvalue spectrum will be too inaccurate because of the uncertainty principle (the resolution of the energy domain is the inverse of the total range covered in the time domain). For instance, if a precision of, say 10 cm^{-1} is desired, one has to propagate up to $\approx$140 000 atomic time units (atu, $1\,\mathrm{atu}=2.419\cdot10^{-17}$ s). Conversely, if the propagation is too long, the probability of having very large prefactors dramatically increases with such an anharmonic potential. The problem clearly demands an optimal compromise. It has been found, by trial and error, that the longest possible propagation not showing chaotic dynamics turned out to be 32 000 atu. This length led to a spectrum with a sufficient precision of 43 cm^{-1}. It is interesting to realize that eigenvalues are much less sensitive to chaoticlike trajectories than eigenvectors. The reason is that since chaos is characterized by motion far from periodic in phase space, its Fourier transform should not preferentially peak to any of the proper frequencies, but rather add a noiselike signal to the entire spectrum. Hence, chaos contamination for the eigenvalues should not be much relevant. Actually, this contamination should quite likely be washed out by the Gaussian filtering. This may be formally seen by considering that the quantum-mechanical autocorrelation function can be expanded in terms of the stationary states as[33]

$$A(t)=\langle\psi(0)|\psi(t)\rangle=\sum_n C_n e^{(-i/\hbar)E_nt}\langle\psi(0)|\Phi_n\rangle$$

$$=\sum_n e^{(-i/\hbar)E_nt}|C_n|^2, \tag{12}$$

so that the Gaussian-filtered energy spectrum, Eq. (10), becomes

$$I(E)=\frac{1}{2\alpha\sqrt{\pi}}\sum_n e^{-(E-E_n)^2/4\alpha^2}|C_n|^2, \tag{13}$$

i.e., a set of Gaussian functions, each centered at each one of the energy eigenvalues. Conversely, eigenvectors are calculated by an integral over the whole time interval on each position over a grid spanning the relevant configuration space. No positions appear to be privileged by the nonchaotic motion, as compared to chaotic, as it happened with the eigenenergies in the energy spectrum. Consequently, the whole eigenvector might be more likely contaminated by the chaotic signature in the time-evolving wave packet.

Once the propagation time length is decided, the next relevant parameter is the number of times the wave packet has to be computed during the propagation. This might be determined by the maximum frequency necessary to be described, since then the Nyquist frequency requirement of the discrete Fourier transform method fixes the value for the sampling rate.[34] For the present system, a maximum frequency of 4000 cm^{-1} proves high enough to describe the bound vibrational states. Hence, the wave packet had to be computed 186 times along the propagation, each one of them separated by a time step of 172 atu.

Finally, the total number of trajectories had to be chosen. Converging the eigenvalue and the eigenvector spectrum required only 8000 bounded trajectories. This number is actually the lowest leading to converged results for the mean position, within a few percent (the test was extended up to 40 000 trajectories). It should be pointed out that since 60% of the trajectories were useless as they ran out from the PES, we needed to start 20 000 trajectories in order to have the above 8000 trajectories remaining inside the bounded region of the PES.

III. NUMERICAL RESULTS AND DISCUSSION

A. PES electronic calculations

An important fraction of the results corresponding to the present electronic calculations have been taken from our previous work.[19(a)] A series of electronic structure calculations were performed to construct a 2D PES. To that purpose, a collection of 80 points, each corresponding to a different set

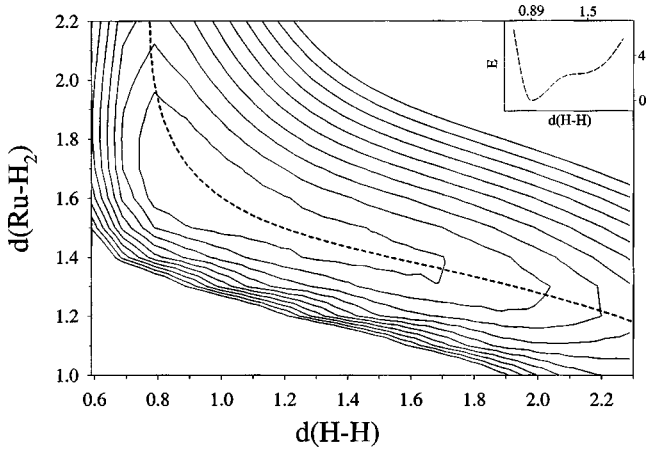

FIG. 2. Contour plot of the two-dimensional potential surface for the complex $[Ru(H\cdots H)(C_5H_5)(H_2PCH_2PH_2)]^+$. Energy contours appear every 4 kcal/mol. Energy profile for the lengthening of the H–H bond, while relaxing the rest of the structure, appears at the top right corner of the figure and projected in the 2D PES (dashed lines). Distances are given in Å and energy in kcal/mol.

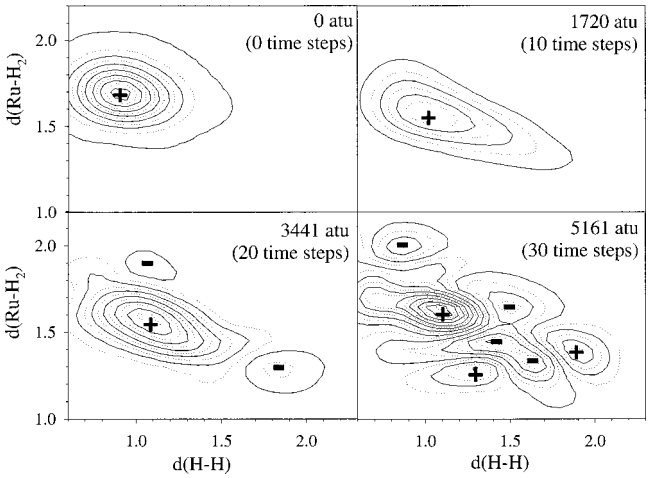

FIG. 3. Snapshots of the time-evolved wave packet at different propagation times. (+) and (−) refer to the sign of the wave packet in order to indicate where the nodes are.

of H–H and Ru–H_2 distances, were calculated. The ranges covered were from 0.59 to 2.29 Å, for the H–H distance (q_1 coordinate), and from 1.0 to 2.2 Å, for the distance between the ruthenium atom and the center-of-mass of the two hydrogen atoms (q_2 coordinate). When calculating the PES global relaxation of the rest of geometrical parameters under C_s symmetry constraint was allowed. The resulting points were fitted to a two-dimensional cubic splines functional form, leading to a smooth and continuous function within the relevant range. This initial set of calculations was then used for an eigenvalue calculation, along with the corresponding vibrational eigenvector determination, by means of the well-known sinc DVR technique.[35]

A further check, shown for the first time in the present work, was performed to ensure that our PES was large enough to properly describe the structural properties of this molecule. It was motivated by the presence of the two exit channels in the PES, and the necessity of knowing the asymptotic regions more accurately (of relevance for the dynamic calculations). This check consisted of an extended PES electronic calculation, which was made by adding to the original PES 54 points calculated by the same methodology. The new range covers from 1.0 to 3.0 Å, along the q_2 coordinate. Calculations showed that no PES enlargement was actually necessary to converge neither the DVR results nor the wave packet semiclassical calculations (see below).

The election of the H–H and Ru–H_2 distances, for the reduced dimensionality 2D PES used in the present study, deserves further comments. These coordinates were chosen as stated since they were found to fulfill two important conditions: (a) they are able to describe properly the dynamics of the H_2 unit of the complex under study (which was the main concern in our previous calculations), and (b) they behave as orthogonal coordinates, thus making diagonal the nuclear kinetic operator (which is a requirement for the DVR method).

Figure 2 depicts the 2D PES as a contour plot. Inspection of this figure discloses two outstanding features of the potential. First, the valley surrounding the minimum energy structure is highly anharmonic. This is a crucial factor in determining the interesting properties of the elongated dihydrogen transition metal complexes, but also a chaos generator, due to the possible instability of a trajectory ensemble. It has to be noted that the values of the H–H and Ru–H_2 distances at the minimum energy structure in the PES are 0.89 and 1.66 Å, respectively. Second, the PES has two exit channels through which the trajectories can escape. Any trajectory whose initial energy is greater than the potential of the edge of the PES in any of the channels, and reaches that channel, will escape from the PES. As we will see in the next section, both features have important consequences for the HK-IVR calculations.

B. HK-IVR calculations

Figure 3 shows some snapshots of the time-evolved wave packet, as obtained from the HK-SC-IVR calculation. It is worthwhile noting the increasingly evident recurrences that appear with increasing time along the propagation. It is well known that these recurrences appear as a consequence of the anharmonicity of the potential. In the present case this is especially suggested after inspection of Fig. 2.

Figure 4 displays the autocorrelation function, while its Fourier transform, after performing Gaussian filtering on it, is depicted in Fig. 5. It thus corresponds to the eigenvalue spectrum of the interaction potential. It specifically displays the peaks corresponding to the three first eigenvalues, out of the just five bounded levels actually supported by the present reduced potential energy surface. The corresponding eigenfunctions are shown in Fig. 6. It is worth noting that these eigenvectors closely match the ones coming from the DVR calculations. Taking into account the experimental conditions in which the structure of the complex was determined by neutron diffraction, as well as a previous DVR calculation, the present result suffices for our purpose. Table I compares the results obtained in the present study with those obtained

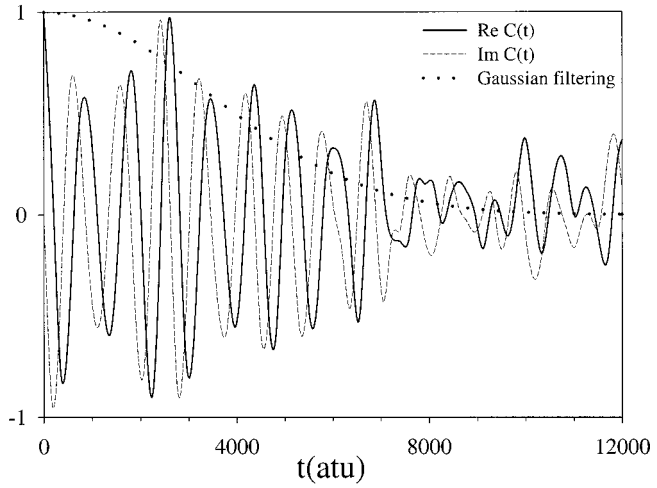

FIG. 4. The real (solid) and imaginary (dashed) parts of the semiclassical correlation function, and the Gaussian filtering (dotted) used for the FFT. A value of $\alpha=(0.5)^{1/2}\cdot(9.5/32000)$, being 32 000 atu the propagation time length, has been used.

by DVR techniques in a previous work;[36] both energy levels and expectation values for the H–H and Ru–H_2 distances are shown.

The highest peak in Fig. 5 corresponds to the zero point energy of the potential energy surface obtained through SC-IVR methods. The SC-IVR result, for the zero point energy and actually for all the energy levels considered, agrees with the DVR reference results within the resolution of the FFT deconvolution. The ability of the SC-IVR methods in particular, and semiclassical methods in general, to reproduce the energy levels for bound systems has been proved several times in the past. However, as analyzed in the previous section, a larger sensitivity to the statistical sampling is expected for the eigenvectors, and hence any quantity directly emerging from them, e.g., the expectation value for the position.

The expectation values for the H–H and Ru–H_2 distances are found to be sufficiently close to the DVR ones, for all energy levels considered. Thus, the availability of the DVR results confirms the correct behavior of the semiclassical method and supports the present choice of a 2D PES for testing purposes. Furthermore, HK-SC-IVR calculations, involving the calculation of the wave function, are affordable since only one phase-space sampling is necessary (contrary to what happens when general correlation functions are needed). Consequently, the present agreement encourages extending the present study to higher dimensionality systems, for which the DVR methodology (or any matrix-based method) is prohibitively expensive. In these cases, though, the use of the SC-IVR would require the formulation of the problem in terms of a regular time-correlation function, to avoid having to store the amplitude of the wave function in the full-dimensional configurational space. In these cases, a double phase-space sampling turns out to be necessary. However, reliable approximate formulations of the SC-IVR suited for calculation of time-correlation functions do exist that would make this endeavor feasible, like the FB-IVR, or the GFB.[1(a),2] This work is to be performed in the near future in our laboratory.

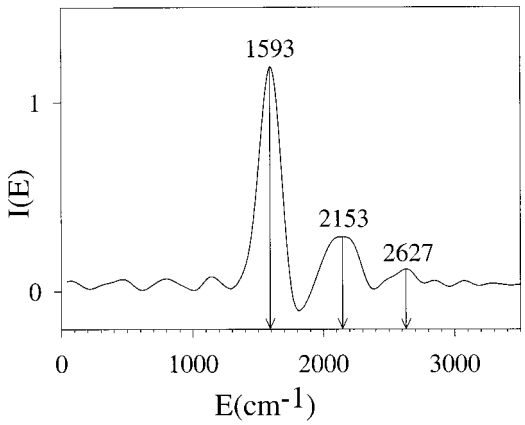

FIG. 5. Eigenvalue spectrum of the interaction potential. Arrows show the energy for the three first eigenvalues.

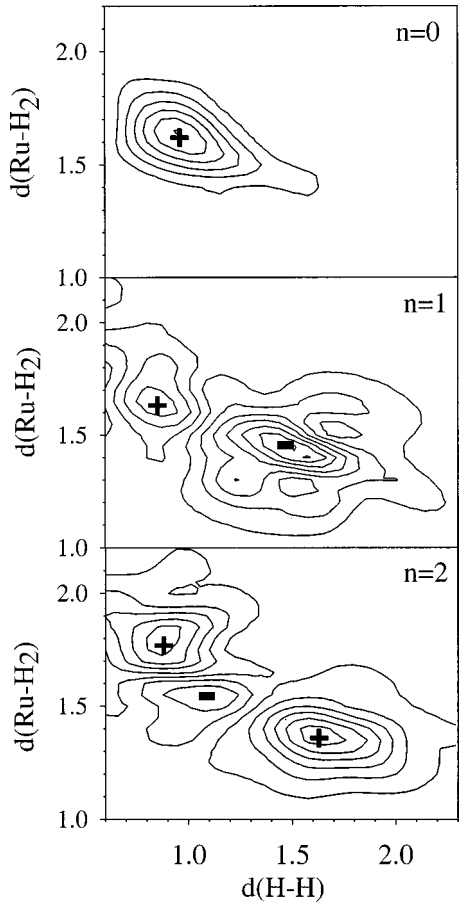

FIG. 6. Eigenfunctions corresponding to the three first eigenvalues $n=0$, 1, and 2. (+) and (−) refer to the sign of the eigenvector in order to indicate where the nodes are.

IV. SUMMARY AND CONCLUSIONS

The molecular geometry mismatch between the predictions by electronic structure theory and the results from neutron diffraction experiments, for the ruthenium dihydrogen complex $[Ru(H\cdots H)(C_5Me_5)(dppm)]^+$, was explained some time ago by Gelabert *et al.*[19(a)] in terms of the wave function delocalization, as a consequence of highly anhar-

TABLE I. Comparison of the SC-IVR and DVR results for the calculation of the three lowest energy levels and expectation values for the H–H and Ru–H_2 distances.

	SC-IVR			DVR[a]		
n	E (cm^{-1})	⟨H–H⟩ (Å)	⟨Ru–H_2⟩ (Å)	E (cm^{-1})	⟨H–H⟩ (Å)	⟨Ru–H_2⟩ (Å)
0	1593±43	1.03	1.60	1579	1.01	1.61
1	2153±43	1.28	1.51	2134	1.27	1.52
2	2627±43	1.37	1.51	2616	1.24	1.55

[a]Data from Ref. 36.

monic potential energy surface. Therefore, it evidences an interesting quantum effect associated to the nuclear motion, since it causes the equilibrium geometry to fall clearly apart from that suggested by electronic structure calculations. This is a strong counterintuitive result from the established chemical point of view.

The present work has addressed the same problem, by means of the semiclassical initial value representation approach, as it prospectively suggested to be a stringent challenge for the methodology: the reduced dimensionality 2D PES features a weakly bound (~20 kcal/mol) species, a strongly anharmonic and coupled surface, as well as two exit channels leading to rearrangement/dissociation. It is, to the best of our knowledge, the first application of the SC-IVR methodology to a molecular geometry problem.

The details of the application run parallel to the eigenvalue calculation for the related PES, i.e., the vibrational spectrum. Hence, the Fourier transform of the autocorrelation function of the time-evolved wave packet becomes the central quantity to be calculated. However, the specific features of the PES required that special care had to be taken with respect to the numerical parameters: (a) the Gaussian wave packet width, as well as the initial position and momenta, were selected so as to lead to the smallest number of runaway trajectories; (b) the propagation time was shortened to avoid dealing with exceedingly large prefactors, but at the same time kept long enough for a sufficiently precise eigenvalue resolution; (c) a comparatively short number of bounded trajectories (~8000) was found to lead to a converged description for both the eigenvalue and the associated vibrational stationary states, even though the latter are quite more sensitive to the statistical sampling than the former.

The present reduced dimensionality problem was chosen since accurate quantum mechanical results could be available, by means of a sinc DVR method, for the eigenvalues, eigenvectors and expectation values for the position of the related dihydrogen bonds. The quantum-semiclassical comparison reveals a nice agreement for the eigenvalues and expectation values, as well as for the overall shape of the eigenvectors, within a few percent. This agreement was clearly expected for eigenvalues, but not quite so for both the eigenvectors and the mean positions. In the near future this result might prompt the extension of the present study to a higher dimensionality PES and, furthermore, to complexes having more than one dihydrogen ligand (or to polyhydride complexes), for which much richer structural features (as well as problems concerning the nuclear symmetry) are expected.

ACKNOWLEDGMENTS

Financial support from the Spanish DGESIC (Project Nos. PB98-0915 and BQU-2001 3018), and the Catalan DURSI (Project Nos. 2001 SGR00048 and 2001 SGR00180) and the use of the computational facilities of the CESCA are gratefully acknowledged.

[1] For recent reviews, see (a) W. H. Miller, J. Phys. Chem. A **105**, 2942 (2001); (b) D. J. Tannor and S. Garaschuk, Annu. Rev. Phys. Chem. **51**, 552 (2000).
[2] H. Wang, D. E. Manolopoulos, and W. H. Miller, J. Chem. Phys. **115**, 6317 (2001).
[3] J. C. Burant and V. S. Batista, J. Chem. Phys. **116**, 2748 (2002).
[4] J. Ankerhold, M. Saltzer, and E. Pollak, J. Chem. Phys. **116**, 5925 (2002).
[5] T. Yamamoto, H. Wang, and W. H. Miller, J. Chem. Phys. **116**, 7335 (2002).
[6] H. Wang, X. Song, D. Chandler, and W. H. Miller, J. Chem. Phys. **110**, 4828 (1999).
[7] S. Garaschuk and D. J. Tannor, Phys. Chem. Chem. Phys. **1**, 1081 (1999).
[8] V. S. Batista, M. T. Zanni, B. J. Greenblatt, D. M. Neumark, and W. H. Miller, J. Chem. Phys. **110**, 3736 (1999).
[9] D. E. Skinner and W. H. Miller, Chem. Phys. Lett. **300**, 20 (1999).
[10] H. Wang, M. Thoss, and W. H. Miller, J. Chem. Phys. **112**, 47 (2000).
[11] H. Wang, M. Thoss, K. L. Sorge, R. Gelabert, X. Giménez, and W. H. Miller, J. Chem. Phys. **114**, 2562 (2001).
[12] R. Gelabert, X. Giménez, M. Thoss, H. Wang, and W. H. Miller, J. Phys. Chem. A **104**, 10321 (2000).
[13] R. Gelabert, X. Giménez, M. Thoss, H. Wang, and W. H. Miller, J. Chem. Phys. **114**, 2572 (2001).
[14] J. Shao and N. Makri, J. Phys. Chem. A **103**, 7753 (1999).
[15] S. Garaschuk and J. C. Light, J. Chem. Phys. **113**, 9390 (2000).
[16] P. R. Wallace, *Mathematical Analysis of Physical Problems* (Dover, New York, 1984).
[17] W. H. Miller, Adv. Chem. Phys. **25**, 69 (1974).
[18] (a) G. J. Kubas, Acc. Chem. Res. **21**, 120 (1988); (b) R. H. Crabtree, *ibid.* **23**, 95 (1990); (c) P. J. Jessop and R. H. Morris, Coord. Chem. Rev. **121**, 155 (1992); (d) D. M. Heinekey and W. J. Oldham Jr., Chem. Rev. **93**, 913 (1993); (e) R. H. Crabtree, Angew. Chem. Int. Ed. Engl. **32**, 789 (1993).
[19] (a) R. Gelabert, M. Moreno, J. M. Lluch, and A. Lledós, J. Am. Chem. Soc. **119**, 9840 (1997); (b) **120**, 8168 (1998).
[20] N. C. Handy, S. M. Colwell, and W. H. Miller, Faraday Discuss. Chem. Soc. **62**, 29 (1977).
[21] X. Sun and W. H. Miller, J. Chem. Phys. **108**, 8870 (1998).
[22] M. J. Frisch, G. W. Trucks, H. B. Schlegel *et al.*, GAUSSIAN 94, Gaussian, Inc., Pittsburgh, PA, 1995.
[23] R. G. Parr and W. Yang, *Density-Functional Theory of Atoms and Molecules* (Oxford University Press, Oxford, 1989).
[24] (a) C. Lee, W. Yang, and R. G. Parr, Phys. Rev. B **37**, 785 (1988); (b) A. D. Becke, J. Chem. Phys. **98**, 5648 (1993).
[25] (a) G. B. Backsay, I. Bytheway, and N. S. Hush, J. Am. Chem. Soc. **118**, 3753 (1996); (b) I. Bytheway, G. B. Backsay, and N. S. Hush, J. Phys. Chem. **100**, 6023 (1996); (c) F. Maseras, A. Lledós, M. Costas, and J. M. Poblet, Organometallics **15**, 2947 (1996); (d) J. Li, R. M. Dickson, and T. Ziegler, J. Am. Chem. Soc. **117**, 11482 (1995); (e) J. Li and T. Ziegler, Organometallics **15**, 3844 (1996); (f) S. Camanyes, F. Maseras, M. Moreno, A. Lledós, J. M. Lluch, and J. Bertrán, J. Am. Chem. Soc. **118**,

4617 (1996); (g) R. Gelabert, M. Moreno, J. M. Lluch, and A. Lledós, Organometallics **16**, 3805 (1997).
[26] P. J. Hay and W. R. Wadt, J. Chem. Phys. **82**, 299 (1985).
[27] W. J. Hehre, R. Ditchfield, and J. A. Pople, J. Chem. Phys. **56**, 2257 (1972).
[28] M. M. Francl, W. J. Pietro, W. J. Hehre, J. S. Binkley, M. S. Gordon, D. J. DeFrees, and J. A. Pople, J. Chem. Phys. **77**, 3654 (1982).
[29] P. C. Hariharan and J. A. Pople, Theor. Chim. Acta **28**, 213 (1973).
[30] X. Giménez, R. Gelabert, and W. H. Miller (unpublished).
[31] K. G. Kay, J. Chem. Phys. **100**, 4377 (1994).
[32] M. D. Feit, J. A. Fleck, Jr., and A. Steiger, J. Comput. Phys. **47**, 412 (1982).
[33] J. Z. H. Zhang, *Theory and Application of Quantum Molecular Dynamics* (World Scientific, Singapore, 1999).
[34] E. Oran Brigham, *The Fast Fourier Transform* (Prentice–Hall, New Jersey, 1974).
[35] D. T. Colbert and W. H. Miller, J. Chem. Phys. **96**, 1982 (1992).
[36] R. Gelabert, M. Moreno, J. M. Lluch, and A. Lledós, Chem. Phys. **241**, 155 (1999).